DTIC FILE COPY

AD-A196 696

REPORT DOCUMENTATION PAGE

READ INSTRUCTIONS
BEFORE COMPLETING FORM

1. REPORT NUMBER	2. GOVT ACCESSION NO.	3. RECIPIENT'S CATALOG NUMBER
AFIT/CI/NR 88- 74		

4. TITLE (and Subtitle)	5. TYPE OF REPORT & PERIOD COVERED
SURFACE TEMPERATURE PREDICTION OF A BRIDGE FOR TACTICAL DECISION AIDE MODELLING	MS THESIS
	6. PERFORMING ORG. REPORT NUMBER

7. AUTHOR(s)	8. CONTRACT OR GRANT NUMBER(s)
PAUL TERRY CROSS, JR.	

9. PERFORMING ORGANIZATION NAME AND ADDRESS	10. PROGRAM ELEMENT, PROJECT, TASK AREA & WORK UNIT NUMBERS
AFIT STUDENT AT: UNIVERSITY OF TENNESSEE - KNOXVILLE	

11. CONTROLLING OFFICE NAME AND ADDRESS	12. REPORT DATE
	1988
	13. NUMBER OF PAGES
	70

14. MONITORING AGENCY NAME & ADDRESS(if different from Controlling Office)	15. SECURITY CLASS. (of this report)
AFIT/NR Wright-Patterson AFB OH 45433-6583	UNCLASSIFIED
	15a. DECLASSIFICATION/DOWNGRADING SCHEDULE

16. DISTRIBUTION STATEMENT (of this Report)

DISTRIBUTED UNLIMITED: APPROVED FOR PUBLIC RELEASE

DTIC
ELECTE
AUG 0 3 1988
D

17. DISTRIBUTION STATEMENT (of the abstract entered in Block 20, if different from Report)

SAME AS REPORT

18. SUPPLEMENTARY NOTES

Approved for Public Release: IAW AFR 190-1
LYNN E. WOLAVER
Dean for Research and Professional Development
Air Force Institute of Technology
Wright-Patterson AFB OH 45433-6583

19. KEY WORDS (Continue on reverse side if necessary and identify by block number)

20. ABSTRACT (Continue on reverse side if necessary and identify by block number)
ATTACHED

8

DD FORM 1473 EDITION OF 1 NOV 65 IS OBSOLETE
1 JAN 73

UNCLASSIFIED

ABSTRACT

An effort was undertaken to develop predictive techniques for determining the surface temperature of a bridge using known or assumed weather data. This type of prediction is useful in Tactical Decision Aide models which are used to provide military field commanders information about guided weapon performance against a particular target. This problem was approached using both one-dimensional and two-dimensional approximations of the Fourier heat equation.

The sensitivity of the model to variations in spatial spacing and time-step, changing diffusivity of the material, and varying lower boundary conditions was examined. Also, the effect of solar side heating on a bridge oriented in a north-south direction as opposed to an east-west oriented bridge was investigated.

iv

A-1

SURFACE TEMPERATURE PREDICTION OF A BRIDGE

FOR TACTICAL DECISION AIDE MODELLING

A Thesis

Presented for the

Master of Science

Degree

The University of Tennessee, Knoxville

Paul Terry Cross, Jr.

June 1987

DEDICATION

This work is dedicated to my father, Paul T. Cross, Sr. It
was at his encouragement that I sought higher education in the
first place. His unselfish attitude in allowing and encouraging
me to attempt all that he thought I was capable of has enabled me
to take advantage of this superior educational opportunity. Most
of all, though, his examples to me of common sense, fairness, hard
work, and righteous living have been an inspiration and will
always guide me in a far deeper way than anything I have learned
here.

ACKNOWLEDGMENTS

In the course of this work, I have been greatly assisted by many. I should first thank my committee: my major professor Dr. Firouz Shahrokhi and Drs. Walter Frost and Ted Paludan. Their kind patience and assistance is greatly appreciated.

Of course, I could not have been here without the support of the U. S. Air Force through the Air Force Institute of Technology. I was also greatly assisted by others associated with the Air Force. They are Lt. Col. Gorden Hammond of the Air Force Geophysics Laboratory; Mr. Dennis Goldstein and Ms. Gini Simpson of the Air Force Armament Laboratory and personnel from their contractor, Analytics, Mr. Ken Krohn, Ms. Pam Ulmer, and Mr. Steven Marlow; and also Capt. Matt Towne, Ms. Martha Simmons and Mr. Robert Hires of the Arnold Engineering Development Center.

The Space Institute Library proved to be an invaluable asset and a bountiful source. I want to particularly thank Ms. Marjorie Joseph who seemed always able to find the reference I needed.

Finally, I want to thank Joyce, my loving wife. She had to endure all my moods, frustrations, and odd hours but still managed to encourage me when I needed it most. This experience has been just as much an education for her as it has been for me.

ABSTRACT

An effort was undertaken to develop predictive techniques
for determining the surface temperature of a bridge using known
or assumed weather data. This type of prediction is useful in
Tactical Decision Aide models which are used to provide military
field commanders information about guided weapon performance
against a particular target. This problem was approached using
both one-dimensional and two-dimensional approximations of the
Fourier heat equation.

The sensitivity of the model to variations in spatial spacing
and time-step, changing diffusivity of the material, and varying
lower boundary conditions was examined. Also, the effect of solar
side heating on a bridge oriented in a north-south direction as
opposed to an east-west oriented bridge was investigated.

TABLE OF CONTENTS

LIST OF TABLES

LIST OF FIGURES

INTRODUCTION

The focus of this research is to develop predictive techniques for determining the surface temperature of bridge-type structures using known or assumed weather data. This technique would be used in Tactical Decision Aide (TDA) models. TDAs are used to provide military field commanders information about the apparent contrast between a target and its background.(Goldman et al, 1983, p.4). Having this information before deployment increases the effectiveness of infrared guided missiles, or helps the field commander make an informed decision about the type of weapons to use.

As used in military research or operations, a TDA consists of three major segments (Ibid). These are prediction of inherent target-to-background contrast, atmospheric effects on the inherent contrast, and sensor response to the apparent contrast. The final result is a predicted acquisition and lock-on range for a specified target, background, and weather history. This research concentrates on the first of these segments.

Contrast predictions of this type have been successfully performed by personnel of the Air Force Armament Laboratory (AFATL) (Goldman et al, 1983). The model for this effort was a one-dimensional Runge-Kutta analysis of the heat flow equations. However, these predictions were typically for small objects such

1

as vehicles or concrete bunkers. Modelling large objects such as bridges presents certain difficulties as noted by Goldman and coworkers.(1983, pp.34-38).

Another related work of this type was by Thepchatri and coworkers in 1977. This effort concentrated on predicting the internal temperature profile of a bridge for the purpose of stress analysis. However, the method used is directly related to this effort because the internal temperature profile is dependent on the surface temperature.

Thepchatri and coworkers used two types of models: a one-dimensional finite difference form of the heat flow equation, and a two dimensional finite element analysis of the heat flow.

I. APPROACH TO THE PHYSICAL PROBLEM

The basic effort here was to determine specific factors
involved in predicting surface temperatures of bridges and develop
an adequate approach for doing so. AFATL had taken radiance
measurements of a bridge in the Destin, FL area, so it was decided
to use this structure to evaluate modelling techniques.

The Destin bridge, shown in Figure 1, runs east-west over a
bay. This provides a constant background which is simpler to
model. Also, because it is an east-west bridge, heating by solar
radiation takes place almost exclusively on the top surface
(Thepchatri et al, 1977, p.40). Since solar radiation is the
dominant energy exchange mechanism, a one-dimensional model was
thought to be adequate to predict the roadway surface temperature.

This hypothesis is further substantiated by thermograph
charts of the Destin bridge (Appendix A) which show the upper
surface of the roadway as the dominant feature, exhibiting the
greatest temperature change throughout a day's cycle. These
thermograph charts are from measurements made by AFATL personnel
on 17 May 1984 (TABILS I). The measurements were made with a AGA
680 Thermovision camera in two wavelength bands: one in the 3.0
to 5.0 micrometer region and the other in the 7.0 to 14.0
micrometer region. The charts in Appendix A are scenes in the

3

Figure 1. Bridge Near Destin, Fl..

4

3.0 to 5.0 micrometer region. The picture in Figure 1 is approximately the scene viewed by the thermovision camera.

Goldman and coworkers (1983, p.35) noted that for structures such as bridges, target recognition may be accomplished by virtue of contrasts within the target. Therefore, in order to study the contrasts within the bridge, it was thought necessary to provide some means of predicting the temperature of these parts of the bridge in addition to the roadway structure.

The thermograph charts indicate that the sides of the roadway and the supporting structure temperatures tend to follow each other. For simplicity, it was decided to model just the vertical piling support underneath the roadway structure and assume that this temperature represented the temperature of the sides also. A schematic of the bridge as modelled is shown in Figure 2.

Modelled in this fashion, the piling model is independent of the model for the roadway surface, which neglects conduction and radiation between the piling and the roadway structure. This is, however, consistent with the conclusions of Goldman and coworkers (1983, p.36) that bridges can be separated into roadway and supporting structures.
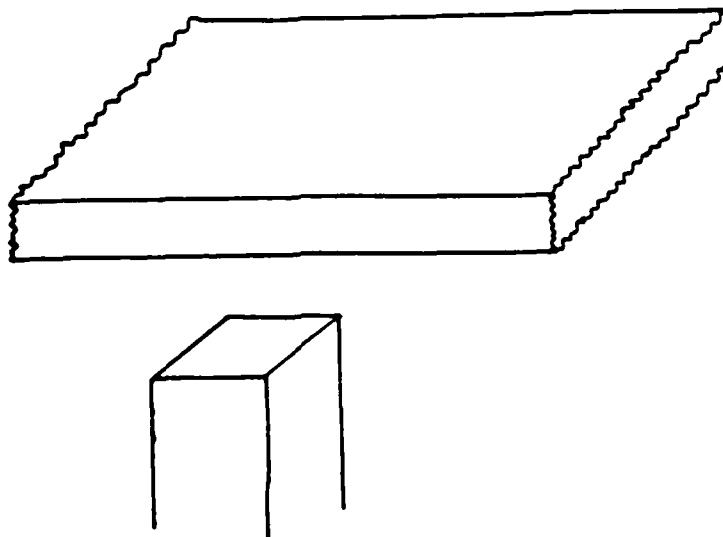
Figure 2. Schematic of Modelled Structure.

A one-dimensional model similar to that used by AFATL to
model vehicles was used to model the Destin bridge, and these
results were compared to temperature data derived from the 17 May
1984 measurements. However, not all bridges will exhibit this
simple geometry, and for bridges running a direction other than
east-west, solar radiation on the sides should be accounted for
using a two-dimensional model (Thepchatri et al, 1977, p.40). For
this reason, a two-dimensional model was used first to model the
Destin bridge in its actual configuration for comparison with
results of the one-dimensional model. Then the Destin bridge was
modelled as if it were at a north-south orientation to determine
the effect of solar loading on the sides.

6

II. MODEL DEVELOPMENT

The models used in earlier studies discussed previously, were based on the Fourier heat conduction equation (Kreith, 1973, p.84),

$$\frac{\partial T}{\partial t} = K\left(\frac{\partial^2 T}{\partial x^2} + \frac{\partial^2 T}{\partial y^2} + \frac{\partial^2 T}{\partial z^2} \right)$$

where t refers to time; x, y, and z refers to the spatial Cartesian coordinates; and K is the thermal diffusivity. This assumes there are no internal heat sources and that the material is isotropic. The equation is subjected to the boundary condition of a heat flux at the surface dependent on the environmental conditions.

Environmental Interactions:

As mentioned above, solar radiation is the dominant energy exchange mechanism affecting surface temperature. However, surface temperature is also influenced by ambient radiation, convection, and conduction to the interior surfaces (Goldman et al, 1983, pp.5-6 and Thepchatri et al, 1977, p.23), with conduction being accounted for by the heat conduction equation.

Goldman and coworkers also mention the contribution of heat transfer by evaporation cooling and condensational heating (1977, p.6), but it is noted that the environmental factor used for this

heat transfer mechanism for concrete is zero (Goldman et al, 1983, p.12). Also, evaporation and condensation are not considered in the models developed by Thepchatri and coworkers. For these reasons, evaporation and condensation were not considered in this effort.

Solar and ambient radiation and convection on a bridge surface are dependent on the local weather conditions. Actual use of a model such as this in an operational military environment will likely have to rely on predicted or estimated weather conditions. Both Goldman and Thepchatri and their coworkers (Goldman et al, 1983, pp.19-27 and Thepchatri et al, 1977, pp.14-18, 23-26) discuss methods of making predictions of the radiation quantities.

For this study, weather data taken in conjuction with the AFATL measurements of the Destin bridge was used. This data was taken over a time period approximately from six o'clock in the morning until midnight on the day of the measurements. The data was taken at approximately one minute intervals with the following quantities being measured: wind speed, wind direction, air temperature, relative humidity, barometric pressure, solar and ambient radiation.

The weather data indicates that the wind was from a generally northerly direction and the velocity was normally 10 knots or less, but occasionally as high as 13 knots. The relative humidity varied from about 20% to as high as 45%, and the barometric pressure varied from about 1021 to 1024 millibars. The variation in air temperature throughout the day is shown in Figure 3, and the variation of the solar and ambient radiation is shown in Figure 4.

The solar and ambient radiation quantities were measured by means of a pyrheliometer and a pyranometer respectively. A pyranometer is a device which measures the total radiation within its hemispherical field of view with the direct beam radiation blocked from the sensor surface by an occulting disk (Kreith and Kreider, 1978, pp.63-66). A pyrheliometer is a similar device which measures the direct beam solar radiation on a horizontal surface while blocking the diffuse sky radiation by mounting the detector at the base of a tube pointed directly at the sun during the day (Ibid).

When the sun is shining on the bridge surface, the heat absorbed by the horizontal surface is given by the intensity of solar radiation, W_{sun}, as measured by the pyrheliometer, multiplied by the solar absorptivity of the surface. The equation (Thepchatri et al, 1977, p.23) is

$$Q_s = \alpha W_{sun}.$$

9
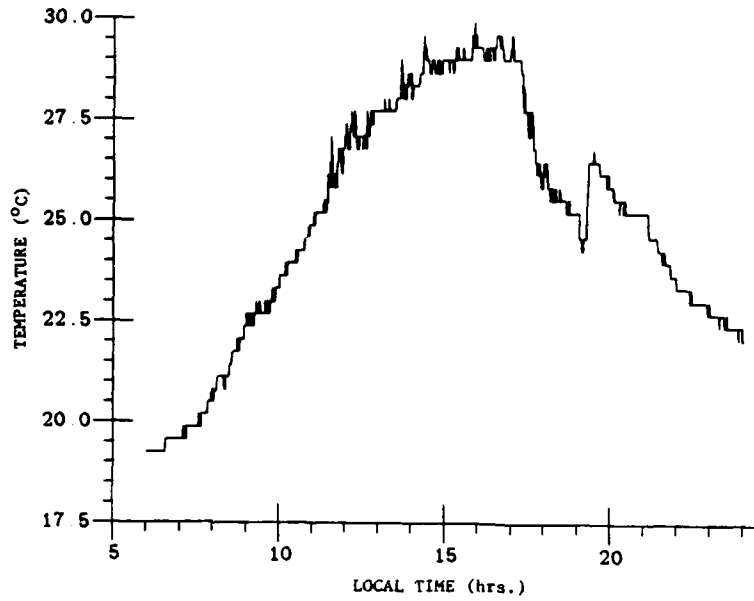
Figure 3. Temperature Cycle for 17 May 1984, Destin, FL.
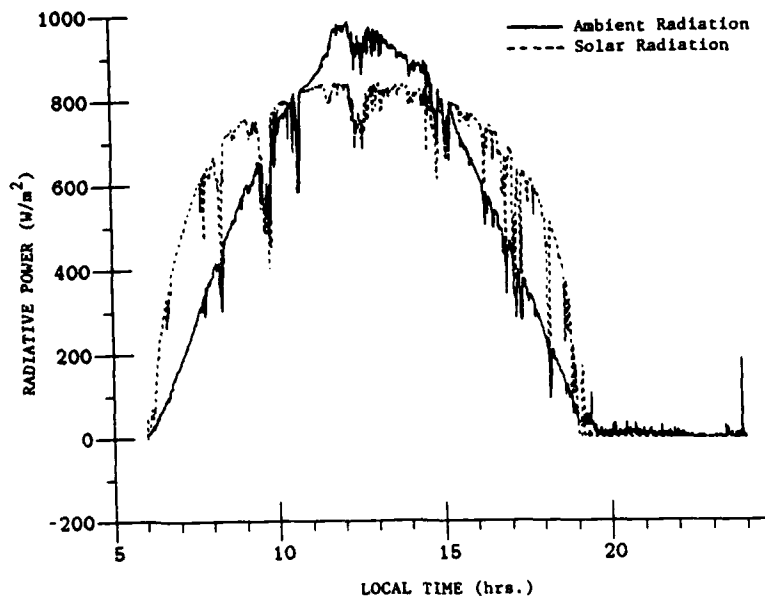
Figure 4. Solar and Ambient Radiation Variation for 17 May 1984, Destin, FL.

10

The solar radiation absorbed is, of course, at a very short wavelength. Radiated heat exchange at longer wavelengths involves a balance between the ambient radiation, W_{sky}, measured by the pyranometer and the emitted radiation of the surface which follows the Stefan-Boltzmann Law (Ibid, p.24). So, given an average emissivity, ϵ, of the surface the heat loss at the top surface to the sky is given by

$$Q_L = \epsilon[\sigma(T_s + 273.15)^4 - W_{sky}]$$

where T_s is the surface temperature of the bridge in degrees Celsius and σ is the Stefan-Boltzmann Constant.

However, the pyranometer measurement will include the contribution of clouds, which absorb radiation during the day and emit it back to the earth during the night (Ibid, p.26). Therefore, for surfaces which do not face the sky, an estimation of the ambient radiation which does not include the cloud contribution is required. This is estimated by applying the Stefan-Boltzmann Law to the ambient air temperature, T_A. Thus, the heat loss to the surroundings from surfaces not facing the sky is given by

$$Q_L = \epsilon\sigma[(T_s + 273.15)^4 - (T_A + 273.15)^4].$$

11

Another major environmental interaction is convection,
including both free and forced convection. At the bridge surface,
this is given by

$$Q_c = (h_1 + h_2 V_A)(T_s - T_A)$$

where V_A is the wind speed and h_1 and h_2 are empirically derived
constants (Ibid, p.27) which are

$$h_1 = 3.775 \ W/m^2\text{-}^oC$$
$$h_2 = 1.689 \ W\text{-}s/m^3\text{-}^oC$$

Another interaction of the bridge with the environment which
sometimes needs to be considered is the reflected and emitted
radiation of the water below. This is a factor which Goldman and
coworkers did not consider because they did not consider objects
with the lower surface open to the environment. Thepchatri and
coworkers (1977, p.61) did make a rough estimate of the reflected
radiation by assuming the bottom surface absorbed 10% of the
incoming solar radiation.

For this analysis, it is assumed that the water reflects the
incoming solar radiation and the ambient radiation and that this
is absorbed by the bridge surface like the ambient radiation when
appropriate. This is given by

12

$$Q_W = \varepsilon r (W_{sun} + W_{sky})$$

where r is the reflectivity of the water. Also note that the average emissivity used for the interaction with the ambient radiation is used here as the absorptivity.

The water also emits radiation, and this is also absorbed like the ambient radiation given as follows

$$Q_E = \varepsilon \varepsilon_w [\sigma (T_w + 273.15)^4]$$

where ε_w is the emissivity of the water and T_w is the temperature of the water in degrees Celsius.

One-Dimensional Model:

The simplest approach to predicting the bridge surface temperature is a numerical approximation of the Fourier equation in one dimension. The two studies which have been discussed here each used slightly different approaches for this approximation. These are briefly discussed in this subsection. However, for the purposes of this study, a one-dimensional model was developed which combines features of the two previously developed models best suited for this purpose or for ease of application.

The model developed by Goldman and coworkers, as previously mentioned, is a Runge-Kutta approximation of the Fourier equation. This is accomplished by first approximating the second order spatial derivative with a finite-difference technique. This yields a system of first order differential equations in time which are solved using the Runge-Kutta technique (Goldman et al, 1983, pp.6-11)

The system of equations results from dividing the structure into layers for application of the finite-difference technique, yielding an equation for each layer. In this case, the solution is for the temperatures at the centers of the layers. The surface temperature is found using a complicated substitution scheme outside the Runge-Kutta loop based on the surface temperature of the previous time, the boundary conditions, and the first layer temperature.

The study by Goldman and coworkers did not discuss modelling the lower boundary open to the air as is the case with a bridge. This can be easily derived, as shown later, by applying the same type of boundary condition on the last layer as is applied on the first.

Thepchatri and coworkers developed a full finite-difference model in both the time and space coordinates (Thepchatri et al, 1977,

14

pp.31-39). In this approach, the structure is also divided into layers but with the temperature solution being at the interface of the layers. The surface temperatures are solved as part of the finite-difference scheme by combining the equations for the heat transfer at the boundaries with the finite-difference equations of the top and bottom layer boundaries.

The model developed for this study used the layer-centered temperature solution and solved the surface tempertures as part of the approximation routine. Figure 5 is a schematic of how this type of structure is applied.
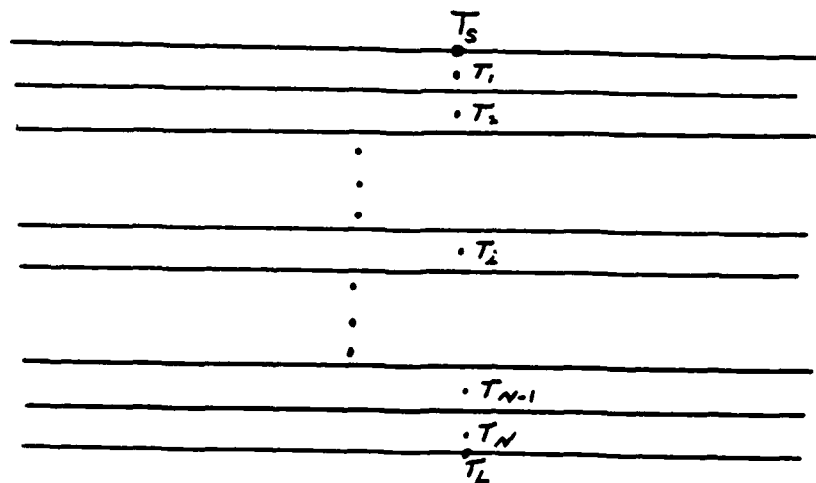
Figure 5. Spacing of Temperature Values in 1-D Model.

In solving for the temperature at the center of a layer of thickness d, the second-order derivative is approximated using a centered-difference form as

$$\frac{\partial^2 T_i}{\partial x^2} = \frac{2}{d^2}(T_{i+\frac{1}{2}d} - 2T_i + T_{i-\frac{1}{2}d}).$$

Using this centered-difference form keeps the calculation of the layer temperature within the layer. Thus, adjacent layers of different materials can be considered without calculating average diffusivity values. However, except for the surface temperatures, only the center layer temperatures are assumed to be known. Thus, the temperatures at the half-steps are assumed to be the average of the temperatures of the two adjacent layers. Applying this to the Fourier equation gives

$$\frac{dT_i}{dt} = \frac{K}{d^2}(T_{i+1} - 2T_i + T_{i-1}).$$

In the top layer, the temperature at $T_{i-\frac{1}{2}d}$ is T_s. So, the approximation to the Fourier equation at T_1 is

$$\frac{dT_1}{dt} = \frac{K}{d^2}(T_2 - 3T_1 + 2T_s).$$

16

Similarly, for the bottom Nth layer where $T_{i+\frac{1}{2}d}$ is T_L, the approximation is

$$\frac{dT_N}{dt} = \frac{K}{c^2}(2T_L - 3T_N + T_{N-1}).$$

Applying this technique to the top surface would give

$$\frac{dT_s}{dt} = \frac{2K}{d^2}(T_1 - 2T_s + T_{s-\frac{1}{2}d}).$$

But, $T_{s-\frac{1}{2}d}$ does not exist. To remedy this, the heat balance at the surface is considered. At the top surface of a roadway structure, this can be expressed as (Thepchatri et al, 1977, p.33)

Heat absorbed from = Heat lost by convection +
short wave radiation   Heat lost by long wave radiation +
                       Heat lost by conduction.

Algebraically, this is

$$\alpha W_{sun} = (h_1 + h_2 V_A)(T_s - T_A) + \epsilon(\sigma(T_s + 273.15)^4 - W_{sky})$$

$$- \frac{k}{d}(T_1 - T_{s-\frac{1}{2}d})$$

where the last term represents the conduction at the surface expressed in centered-difference form, with k being the thermal conductivity. Solving this expression for $T_{s-\frac{1}{2}d}$ and substituting

17

that into the approximation of the Fourier equation at the top
surface gives

$$\frac{dT_s}{dt} = \frac{4\alpha_5}{d^2}(T_1 - T_2) + 2W(T_s)$$

where

$$W(T_s) = \frac{\alpha_1}{d}W_{sun} + \frac{\alpha_2}{d}[W_{sky} - \sigma(T_s + 273.15)^4]$$
$$+ (\frac{\alpha_3}{d} + \frac{\alpha_4}{d}V_A)(T_A - T_s).$$

The alpha terms are environmental constants the same as those
derived by Goldman and coworkers (1983, pp.7-8). These are

$$\frac{\alpha_1}{d} = \frac{\alpha}{\rho c d}$$

$$\frac{\alpha_2}{d} = \frac{\varepsilon}{\rho c d}$$

$$\frac{\alpha_3}{d} = \frac{h_1}{\rho c d}$$

$$\frac{\alpha_4}{d} = \frac{h_2}{\rho c d}$$

$$\frac{\alpha_5}{d^2} = \frac{k}{\rho c d^2}.$$

A similar scheme is used at the lower surface of the roadway
structure, where the heat balance is (Thepchatri et al, 1977, p.33)

18

Heat gained by conduction   Heat lost by convection +
+ Heat gained from water = Heat lost by long wave
     radiosity   radiation.

Algebraically, with the conduction term expressed in the same

manner as for the top surface, this is

$$\frac{k}{d}(T_N - T_{L+\frac{1}{2}d}) + \varepsilon r(W_{sun} + W_{sky}) + \varepsilon \varepsilon_w \sigma (T_w + 273.15)^4$$

$$= (h_1 + h_2 V_A)(T_s - T_A)$$

$$+ \varepsilon \sigma [(T_s + 273.15)^4 - (T_A + 273.15)^4].$$

Solving for $T_{L+\frac{1}{2}d}$ and substituting into the Fourier equation gives

$$\frac{dT_L}{dt} = \frac{4\alpha_5}{d^2}(T_N - T_L) + 2W(T_L)$$

where

$$W(T_L) = \frac{\alpha_2}{d}[(T_A + 273.15)^4 - (T_s + 273.15)^4]\sigma + E_w$$

$$+ (\frac{\alpha_3}{d} + \frac{\alpha_4}{d}V_A)(T_A - T_s) + \frac{\alpha_6}{d}(W_{sun} + W_{sky}).$$

Additional environmental constants in this case are as follows:

$$E_w = \frac{\varepsilon_w \varepsilon}{\rho c d}(T_w + 273.15)^4 \sigma$$

$$\frac{\alpha_6}{d} = \frac{\varepsilon r}{\rho c d}$$

19

It is important to note here that the emitted and reflected radiation of the water is applied only to the lower surface as would be the case for the roadway. Specific applications will determine exactly when the various environmental constants should be applied.

This system of expressions for the Fourier equation can be used with the Runge-Kutta method to obtain solutions of the time derivatives. This is done for this study using the Runge-Kutta method of order four (Burden and Faires, 1985, pp.263-265). In this case, the equations are

$$F_s = 4\frac{\alpha_5}{d^2}(T_1 - T_s) + 2W(T_s)$$

$$F_1 = \frac{\alpha_5}{d^2}(T_2 - 3T_1 + 2T_s)$$

$$F_i = \frac{\alpha_5}{d^2}(T_{i+1} - 2T_i + T_{i-1})$$

$$F_N = \frac{\alpha_5}{d^2}(2T_L - 3T_N + T_{N-1})$$

$$F_L = 4\frac{\alpha_5}{d^2}(T_N - T_L) + 2W(T_L).$$

An initial approximation, T_{i0}, for each temperture is assumed. Then, if the time increment is h and with T_{ij} representing the ith temperature at the jth time increment, the

20

ith temperature at the next time increment is obtained by first
calculating

$$k_{1i} = hF_i(t_j, T_{sj}, T_{1j}, \ldots, T_{Lj})$$

$$k_{2i} = hF_i(t_j + \frac{h}{2}, T_{sj} + \tfrac{1}{2}k_{1s}, \ldots, T_{Lj} + \tfrac{1}{2}k_{1L})$$

$$k_{3i} = hF_i(t_j + \frac{h}{2}, T_{sj} + \tfrac{1}{2}k_{2s}, \ldots, T_{Lj} + \tfrac{1}{2}k_{2L})$$

$$k_{4i} = hF_i(t_j + h, T_{sj} + k_{3s}, \ldots, T_{Lj} + k_{3L}).$$

Then the solution at the next time increment is

$$T_{i,j+1} = T_{ij} + [k_{1i} + 2k_{2i} + 2k_{3i} + k_{4i}]/6.$$

The time derivatives can also be expressed in
finite-difference form, which gives the following system of
equations:

$$T_s' = T_s + 4h\frac{\alpha_5}{d^2}(T_1 - T_s) + 2hW(T_s)$$

$$T_1' = T_1 + h\frac{\alpha_5}{d^2}(T_2 - 3T_1 + 2T_s)$$

$$T_i' = T_i + h\frac{\alpha_5}{d^2}(T_{i+1} - 2T_i + T_{i-1})$$

$$T_N' = T_N + h\frac{\alpha_5}{d^2}(2T_L - 3T_N + T_{N-1})$$

$$T_L^- = T_L + 4h\frac{\alpha_5}{d^2}(T_N - T_L) + 2hW(T_L)$$

where h is again the finite time increment and the prime
represents the new temperature at the end of the time step. Both
the Runge-Kutta Method and the full finite-difference method were
used in this analysis for comparison.

Two-Dimensional Model:

A two-dimensional model was developed to study what effect
solar loading on more than one side might have on the surface
temperature. This situation is significant when the bridge
is at an orientation other than east-west and would be
particularly significant on smaller parts of the bridge such as
the vertical pilings.

Thepchatri and coworkers (1977, p.40) noted that a
two-dimensional model would be necessary for temperature
prediction of bridges at other than an east-west orientation.
They developed a finite-element model for their analysis, but for
the purposes of this study, a finite-element analysis was thought
to be too intensive.

Application of the TDA models in the field, very often on
hand-held computers (Wachtmann et al, 1985, p.15), would preclude
use of a model requiring large amounts of memory or program

22

instructions as a finite-element model would. However, it is important to know the effect of solar side-heating and determine if the one-dimensional model adequately predicts the surface temperature.

For the purposes of this study, it was decided to develop a simple finite-difference two-dimensional model to study the effects of solar side-heating and for application to a TDA model if appropriate. This development involves simply applying the finite-difference technique to two coordinates of the Fourier equation, which gives

$$T'_{ij} = T_{ij} + \frac{Kh}{d_x^2}(T_{i+1,j} - 2T_{ij} + T_{i-1,j})$$
$$+ \frac{Kh}{d_y^2}(T_{i,j+1} - 2T_{ij} + T_{i,j-1})$$

where d_x, d_y, and the T_{ij}s are as shown in Figure 6. If this equation is developed as the one-dimensional model, for the temperatures on the far left of the slab, the following equations are obtained:

$$T'_{11} = T_{11} + 4h\frac{\alpha_5}{d_x^2}(T_{21} - T_{11}) + 2hW_x(T_{11})$$

$$+ 4h\frac{\alpha_5}{d_y^2}(T_{12} - T_{11}) + 2hW_y(T_{11})$$

23

$$T'_{21} = T_{21} + h\frac{\alpha_5}{d_x^2}(T_{31} - 3T_{21} + 2T_{11})$$

$$+ 4h\frac{\alpha_5}{d_y^2}(T_{22} - T_{12}) + 2hW_y(T_{21})$$

$$T'_{i1} = T_{i1} + h\frac{\alpha_5}{d_x^2}(T_{i+1,1} - T_{i1} + T_{i-1,1})$$

$$+ 4h\frac{\alpha_5}{d_y^2}(T_{i2} - T_{i1}) + 2hW_y(T_{i1})$$

$$T'_{N-1,1} = T_{N-1,1} + h\frac{\alpha_5}{d_x^2}(2T_{N1} - 3T_{N-1,1} + T_{N-2,1})$$

$$+ 4h\frac{\alpha_5}{d_y^2}(T_{N-1,2} - T_{N-1,1}) + 2hW_y(T_{N-1,1})$$

$$T'_{N1} = T_{N1} + 4h\frac{\alpha_5}{d_x^2}(T_{N-1,1} - T_{N1}) + 2hW_x(T_{N1})$$

$$+ 4h\frac{\alpha_5}{d_y^2}(T_{N2} - T_{N1}) + 2hW_y(T_{N1}).$$
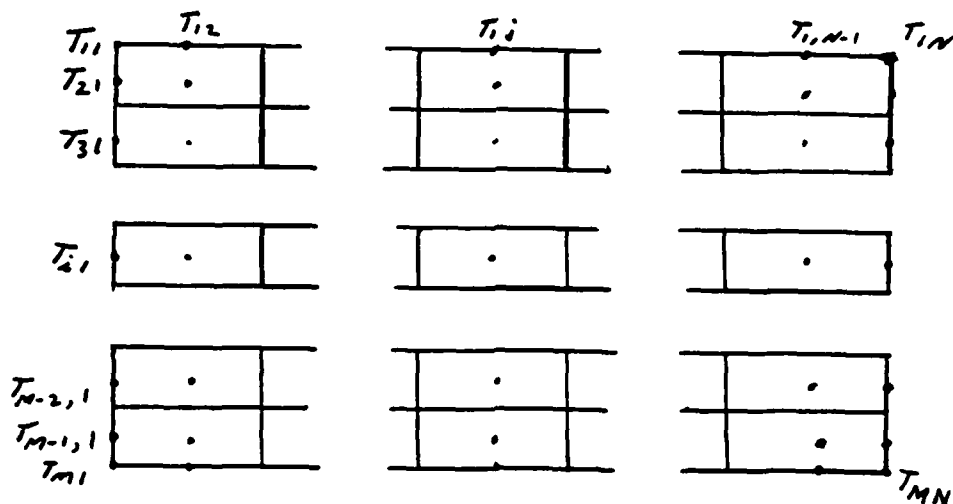
Figure 6. Spacing of Temperature Values in 2-D Model.

24

Calculation of the next column of temperatures to the right would
involve using a y-component of the equation similar to the
x-component of the second equation above. The y-component would
continue to change similarly for each succeeding column to the
right.

III. SENSITIVITY ANALYSIS

In order to properly apply the modelling techniques to the physical problem, it was necessary to study the impact of various factors. Factors such as the sensitivity of the models to changes in the finite time step and spatial step, key physical properties, and certain environmental interactions were investigated. Also, the impact of the two different approximation techniques was considered. These sensitivity analyses were performed using the one-dimensional roadway structure model.

Physical properties used in performing these analyses were obtained from the work by Thepchatri and coworkers (1977, p.60). These are

Absorptivity of Surface to Solar Radiation	0.5
Emissivity	0.9
Density	150 lbm/ft^3 2403 kg/m^3
Thermal Conductivity	0.81 Btu/ft/hr/$^{\circ}$F 1.4 W/m/$^{\circ}$C
Specific Heat	0.23 Btu/lbm/$^{\circ}$F 963 W-s/kg/$^{\circ}$C

Generally, these models were set up as if reflected radiation from the water was incident on the lower surface of the bridge. When emitted radiation was also considered, the water was assumed

26

to be at a constant temperature throughout the day. Based on informal studies (Marlow, 1986) this temperature was chosen to be 22°C. The reflectivity and emissivity of the water were assumed to be 0.05 and 0.95 respectively (Wolfe and Zissis, 1978, p.3-106).

It was also necessary to choose an initial temperature profile for the bridge. Based on previous studies (Thepchatri et al, 1977, p.60), the initial temperature profile of the bridge was assumed to be constant and at the ambient air temperature at the start time. This initial temperature was 19.25°C at the starting time of the prediction, 6:07 AM.

Time and Spatial Sensitivity:

In any finite-difference technique, the size of the finite steps is important. Too large a step-size results in unacceptable inaccuracies while too small of a step may require an excessive amount of computer run time. The key is to find the largest step-size which gives an acceptable degree of accuracy.

Another consideration with the models developed here is choosing a combination of time and spatial step-sizes which will not result in numerical instabilities. In this case, numerical instabilities will result when the quantity

$$T_s - 4h\frac{\alpha_s}{d^2}T_s$$

27

becomes less than zero. Therefore to avoid numerical

instabilities the time step and layer thickness should be selected

such that

$$4h\frac{\alpha_s}{d^2} < \frac{1}{4}.$$

To investigate the sensitivity of the models to variations in

time-step, a three layer model of the roadway structure was used.

Since the roadway structure is 7.5 inches thick (see schematics in

Appendix B), this gives a layer thickness of 2.5 inches, or 0.0635

meters. Time-steps of one, five, ten, and fifteen minutes were

compared.

The results of the time-step sensitivity analysis are given

in Table 1, which displays the results in increments of one hour

after the initial time. This shows very little change as the

time-step is varied from one to 15 minutes, with the variation in

temperature always being less than two degrees Celsius and most

of the time less than one degree. It is interesting to note,

however, that the maximum difference in the magnitude of the peak

temperatures is less than 0.6°C.

Table 1 also shows consistent results between the Runge-Kutta

and the finite-difference models, with differences at a given time

and time-step for the most part being less than one degree

Celsius (with one notable exception at 19:07 using a 15 minute

TABLE 1

TIME SENSITIVITY USING 3-LAYER MODEL

					TEMPERATURES - °C				
TIME STEP	1 MIN		5 MIN		10 MIN		15 MIN	
MODEL TYPE	F-D	R-K	F-D	R-K	F-D	R-K	F-D	R-K
TIME								
7:07	17.56	17.54	17.44	17.27	17.20	16.81	17.04	16.45
8:07	22.91	22.86	22.83	22.57	22.69	22.13	22.54	21.62
9:07	29.37	29.31	29.35	29.01	29.29	28.57	28.89	27.72
10:07	34.33	34.27	34.47	34.12	33.80	33.30	35.29	34.01
11:07	41.78	41.71	41.89	41.50	42.33	41.56	42.23	41.11
12:07	49.32	49.25	49.29	48.92	49.57	48.79	49.54	48.30
13:07	52.97	52.92	53.23	53.00	53.23	52.75	54.07	53.06
14:07	55.54	55.52	55.95	55.82	56.10	55.81	56.87	56.33
15:07	55.78	55.77	56.13	56.06	56.50	56.37	54.67	55.25
16:07	54.93	54.92	54.94	54.95	55.00	55.02	54.74	54.90
17:07	50.77	50.80	50.96	51.12	50.60	51.17	50.75	51.50
18:07	44.25	44.30	44.65	44.85	44.99	45.51	44.64	45.26
19:07	35.19	35.27	35.17	35.63	36.35	37.18	34.69	36.54
20:07	27.66	27.71	27.63	27.91	28.04	28.63	27.58	28.49
21:07	23.24	23.28	23.20	23.39	23.46	23.86	23.14	23.75
22:07	19.83	19.87	19.80	19.97	20.03	20.38	19.68	20.24
23:07	17.20	17.23	17.22	17.34	17.31	17.60	17.13	17.58
23:57	15.59	15.61	15.46	15.58	15.62	15.86	*15.58	*15.93
TIME OF PEAK TEMP.	14:41	14:41	14:47	14:47	14:37	14:37	14:07	14:52
PEAK TEMP.	56.33	56.30	56.48	56.39	56.85	56.53	56.87	56.46

*FINAL TEMPERATURES FOR 15 MINUTE TIME-STEP ARE AT 23:52.

29

time step where the difference is $1.85^{\circ}C$). For the five minute
and one minute time-steps, the difference between the two models
is less than $0.5^{\circ}C$.

The time of occurence of the peak temperature varies as the
time-step varies but is consistent between the two models except
for the 15 minute time step. The variation in the peak occurence
is small for the time-steps up to 10 minutes and could be a result
of the coarseness of the models. The time of the peak using the
15 minute time-step with the Runge-Kutt* model is also reasonably
close to the other time-steps, but the 15 minute,
finite-difference result is too far removed from the other results.

To study the sensitvity of the models to variations in layer
thickness, a one minute time-step was used with three, five, ten,
and fifteen layer models. Again, both the Runge-Kutta and
finite-difference models were investigated. Layer thicknesses
corresponding to the number of layers used are 0.0636 m, 0.0381 m,
0.0190 m, and 0.0127 m respectively. It should also be noted that
15 layers is the most that can be used with a one minute time-step
and avoid numerical instabilities with this model and the given
physical properties. A smaller time step could be used with more
layers, but one minute was the minimum used in this study because
the weather data availabe was given at approximately one minute
intervals.

Table 2 shows the results of the spatial sensitivity study. These results indicate that varying the number of layers produces a greater variation in the temperature prediction than varying the time-step. In this case, a variation of as much as four degrees Celsius is seen occuring at 13:07. However, the variation is less than two degrees if the three layer model is not considered. Also, the variation in the magnitude of the peak temperature is as much as 2.75°C, but only 1.4°C if the three layer model is not considered. If just the ten and 15 layer models are considered, the variation is less than 0.5°C. It is also noted that the time of occurence of the peak is consistent with all the models used in the spatial sensitivity study.

The consistency between the finite-difference and the Runge-Kutta models is better as the number of layers is varied than if the time-step is varied. The data from Table 2 indicates that for a given number of layers the variation between the two models at any time is less than 0.12°C.

The results of the time and spatial sensitivity studies indicate that reasonable accuracy can be obtained with either the finite-difference or the Runge-Kutta model. However, to maintain the accuracy, the time-step should be less than five minutes and the number of layers should be greater than five. For further sensitivity studies, only the finite-difference model was used.

31

TABLE 2

SPATIAL SENSITIVITY USING [?] MINUTE TIME-STEP

------ TEMPERATURES - °C ------

NO. LAYERS	3		5		10		15	
TYPE MODEL	F-D	R-K	F-D	R-K	F-D	R-K	F-D	R-K
TIME								
7:07	17.56	17.54	17.64	17.61	17.67	17.63	17.74	17.67
8:07	22.91	22.86	23.40	23.34	24.01	23.93	24.28	24.19
9:07	29.37	29.31	30.29	30.21	31.28	31.19	31.70	31.58
10:07	34.33	34.27	35.63	35.53	36.72	36.63	37.13	37.05
11:07	41.78	41.71	43.31	43.22	44.71	44.63	45.26	45.18
12:07	49.32	49.25	51.06	50.99	52.68	52.60	53.26	53.20
13:07	52.97	52.92	54.57	54.53	55.93	55.87	56.42	56.32
14:07	55.54	55.52	56.84	56.84	57.77	57.82	58.09	58.14
15:07	55.78	55.77	56.96	56.95	57.68	57.72	57.86	57.96
16:07	54.93	54.92	55.79	55.80	56.32	56.33	56.47	56.49
17:07	50.77	50.80	51.26	51.26	51.38	51.41	51.31	51.37
18:07	44.25	44.30	44.05	44.11	43.60	43.65	43.47	43.42
19:07	35.19	35.27	34.23	34.34	33.12	33.22	32.63	32.73
20:07	27.66	27.71	26.67	26.73	25.56	25.61	25.17	25.18
21:07	23.24	23.28	22.22	22.26	21.25	21.29	20.90	20.95
22:07	19.83	19.87	18.85	18.88	17.97	18.00	17.64	17.70
23:07	17.20	17.23	16.29	16.31	15.52	15.54	15.30	15.27
MIDNIGHT	15.48	15.50	14.63	14.66	13.93	13.95	13.72	13.71
TIME OF PEAK TEMP.	14:41	14:41	14:41	14:41	14:41	14:41	14:41	14:41
PEAK TEMP.	56.33	56.30	57.68	57.65	58.68	58.66	59.05	58.98

Sensitivity to Changing Diffusivity:

Concrete bridges such as the one considered here typically have steel reinforcements. The amount of steel used in any particular bridge may vary, which would greatly alter the diffusivity factor used in the model. This results because the thermal conductivity of steel is on the order of 30 times greater than that of concrete, while the product of the density and specific heat of steel is only about 1.6 times greater than that of concrete.

For example, average values of concrete thermal properties applicable to steel reinforced bridges are (Thepchatri et al, 1977, p.60)

Thermal conductivity	0.81 Btu/ft/hr/$^{\circ}$F
	1.4 W/m/$^{\circ}$C
Density	150 lb/ft^3
	2403 kg/m^3
Specific heat	0.23 Btu/lb/$^{\circ}$F
	963 W-s/kg/$^{\circ}$C

Comparable values for steel are (Rohsenow and Hartnett, 1973, pp.2-67,68)

Thermal conductivity	26.6 Btu/ft/hr/$^{\circ}$F
	46 W/m/$^{\circ}$C
Density	500 lb/ft^3
	8009 kg/m^3
Specific heat	0.11 Btu/lb/$^{\circ}$F
	460 W-s/kg/$^{\circ}$C

As used in the model, the surface properties of the bridge are all divided by the product of the density and specific heat.

33

However, this product is very large for both concrete and steel while the surface properties are relatively very small numbers. From this it was concluded that the effect of varying amounts of steel in the bridge struture would be almost entirely from the diffusivity term.

Therefore, to study this effect, the model was run for cases where the diffusivity term is multiplied by factors of two, five, and eight. A five layer, one minute time-step model was used. The one minute time-step was selected to avoid numerical instabilities with the larger diffusivity terms.

Table 3 shows the results of this analysis. The magnitude and time of occurence of the peak temperature is of most significance here. It can be seen that the peak temperature is reduced by almost nine degrees Celsius when the diffusivity is eight times its normal value, and the time of the peak is delayed until almost 1.3 hours later. Also, the results using a factor of five are very close to those obtained using a factor of eight, indicating a leveling-out of this effect. A slight lowering of the peak temperature without shifting the time of occurence is obtained using a factor of two times the diffusivity.

The effect of changing diffusivity is shown graphically in Figure 7 where the resulting temperatures for cases of one times

TABLE 3
SENSITIVITY TO CHANGING DIFFUSIVITY

DIFFUSIVITY	--------- TEMPERATURES - ^{o}C ---------			
FACTOR	1X	2X	5X	8X
TIME				
7:07	17.64	17.90	18.26	18.41
8:07	23.40	22.57	21.69	21.30
9:07	30.29	28.30	26.12	25.26
10:07	35.63	32.93	30.02	28.98
11:07	43.31	39.44	35.42	34.01
12:07	51.06	46.13	41.14	39.44
13:07	54.57	49.72	44.90	43.34
14:07	56.84	52.30	47.89	46.48
15:07	56.96	53.10	49.37	48.21
16:07	55.79	52.66	49.76	48.88
17:07	51.26	49.49	47.92	47.51
18:07	44.05	43.85	43.96	44.10
19:07	34.23	35.86	37.68	38.40
20:07	26.67	29.33	32.17	33.21
21:07	22.22	25.14	28.08	29.06
22:07	18.85	21.76	24.57	25.46
23:07	16.29	19.01	21.56	22.37
MIDNIGHT	14.63	17.10	19.39	20.14
TIME OF				
PEAK TEMP.	14:41	14:41	16:02	16:08
PEAK TEMP.	57.68	53.39	49.80	48.91

NOTE: TEMPERATURES MODELLED USING 1 MINUTE TIME-
STEP, 5-LAYER, FINITE-DIFFERENCE MODEL.
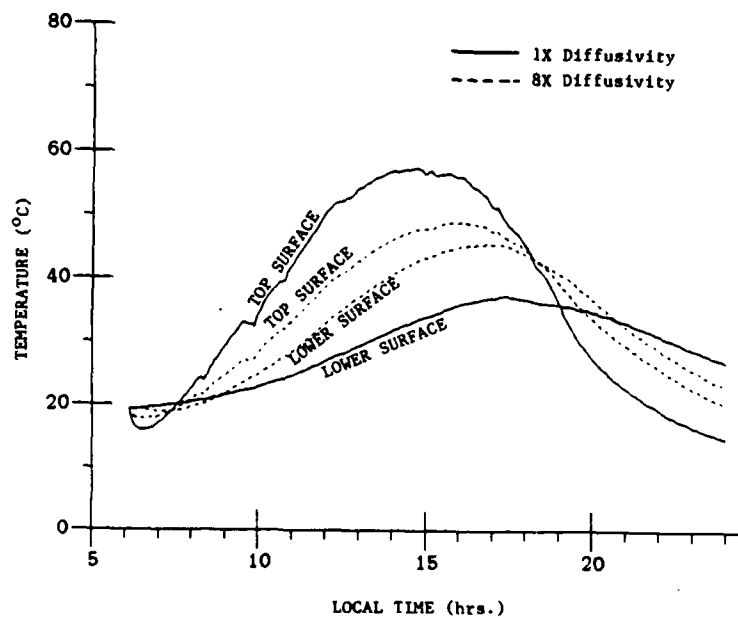
Figure 7. Effect of Changing Diffusivity on Surface Temperatures
with Reflected Radiation only Incident on Lower Surface.

and eight times the diffusivity are plotted against time. Both
the top surface and lower surface temperatures are plotted to show
how they approach each other more closely with a higher
diffusivity.

The shifting of the peak is likely due to the effect of the
radiation incident on the lower surface. This incident radiation
serves to heat the lower surface, and with the higher diffusivity,
this heat is more readily conducted to the top surface. The model
used for this sensitivity analysis considered only reflected
radiation from the water onto the lower surface. Varying effects
of radiation incident on the lower surface were also considered.

Lower Boundary Sensitivity:

Variations in the surroundings or structure of a particular
bridge may affect the amount of radiation received by its lower
surface. In the sensitivity analyses discussed so far, the models
considered only reflected radiation from the water incident on the
lower surface. However, radiation emitted by the water may
greatly impact the radiation heat transfer to the lower surface,
or the structure may be such that no radiation from the
surroundings is incident on the lower surface.

For most TDA applications, the temperature of the lower
surface is of no consequence except, as shown in the previous

36

subsection, for how it affects the top surface temperature.
Therefore, it is important to know how varying amounts of
radiation from the surroundings incident on the lower surface will
affect the top surface temperature.

To study this effect, the finite-difference model was run for
cases of no radiation, reflected radiation only, emitted radiation
only, and both reflected and emitted radiation incident on the
lower surface. To see the relation of the top surface temperature
with that of the lower surface, the results of these cases are
shown in graphical form in Figures 7 - 10 where both the top and
lower surface temperatures are plotted for each case.
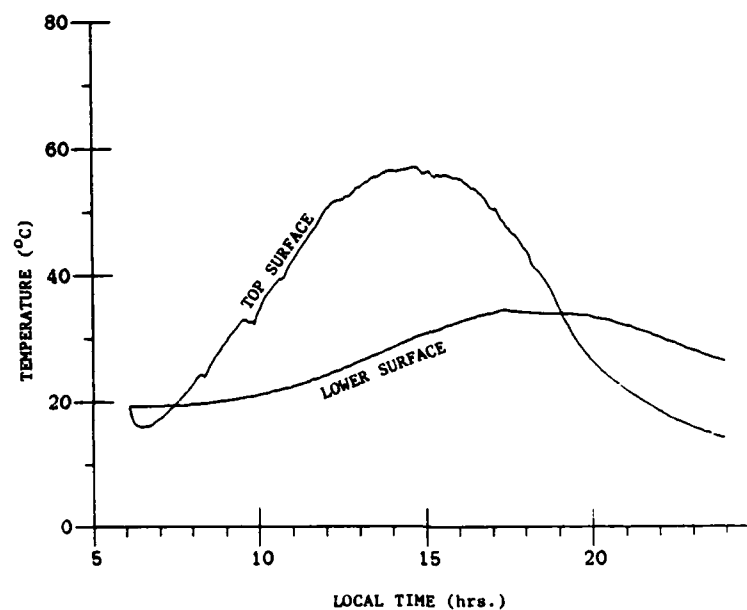
Figure 8. Effect of No Radiosity Incident on Lower Surface.
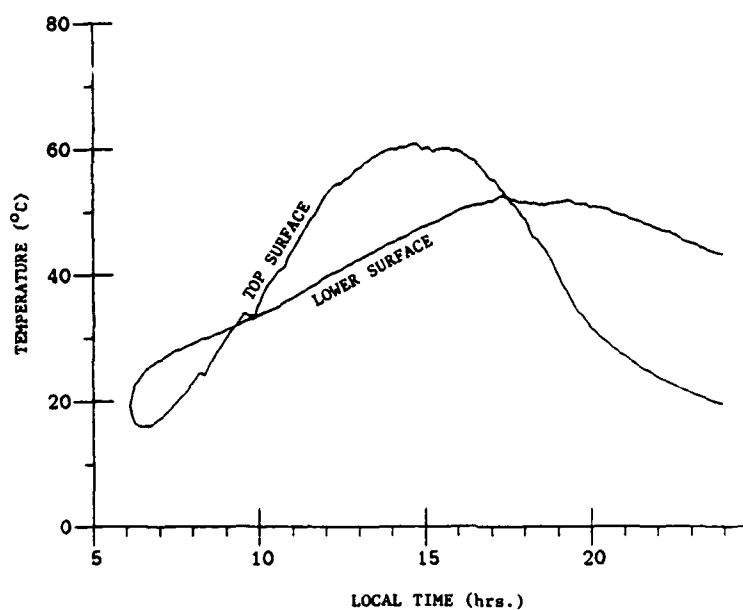
Figure 9. Effect of Emitted Radiation only Incident on Lower
Surface.
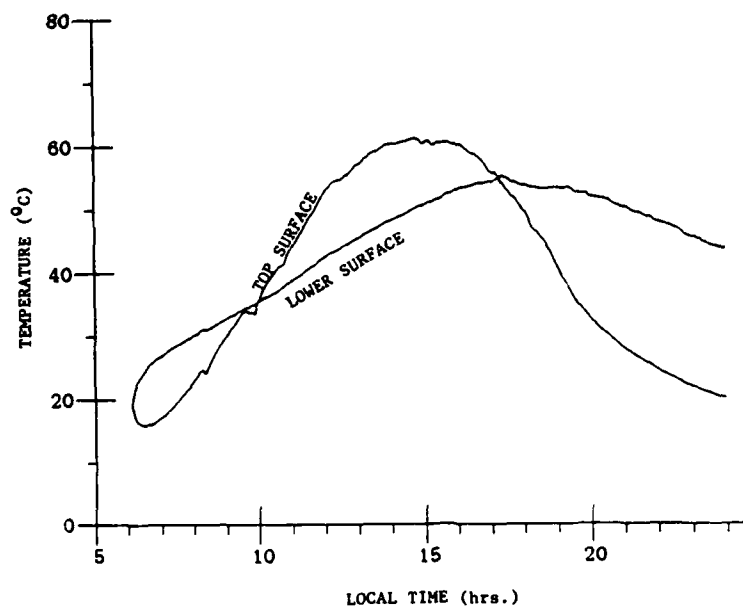
Figure 10. Effect of Emitted and Reflected Radiation Incident on
Lower Surface.

38

It is noted from these figures that large increases are seen in the lower surface temperatures (as much as 20°C for the extreme cases). However, the increase in the top surface temperature is only about four degrees Celsius.

IV. MODELLING RESULTS

An appropriate form of the one-dimensional finite-difference
model was selected to make a prediction of the bridge surface
temperatures for the day of the measurements. The selection of
this model was based on the results of the sensitivity analyses
and estimates of the surface temperatures made from the radiance
measurements. Using this prediction as a baseline, a
two-dimensional finite-difference model was also used to predict
the surface temperature distribution for comparison to the
one-dimensional results. The two-dimensional model was also used
to investigate the side-heating impact of a north-south oriented
bridge. Sample program listings for both the one-dimensional and
two-dimensional models can be found in Appendix C.

Just one of the developed one-dimensional models was carried
through this process based on the results of the sensitivity
analyses. These showed that the variation between results of the
two models was insignificant provided the proper time and spatial
spacing was used. The finite-difference model was selected
because it is more straight-forward and easier to implement. This
model was used with a five minute time-step and five layers, and
again the starting time was 6:07 AM and the initial temperature
distribution was assumed to be a constant $19.25^{\circ}C$.

Estimates of Actual Temperatures:

The radiance measurements made by AFATL on 17 May 1984 (TABILS I) provided a means to estimate the actual temperatures of the bridge. Scenes of the bridge in the 7.0 to 14.0 micrometer band taken at various times during the day were analyzed using the process described by Goldman and coworkers (1983, pp.50-53). This process provided a value for the radiance at the detector, I_D. Using the weather data taken on the day of measurements and the system spectral response, a transmittance value, t, combining the path transmittance and system spectral response was found. Also, a value for the radiance of the path, I_P, was found using the weather data.

With an estimate of these values, the radiance at the source, I_S, could be estimated. This is given by

$$I_S = \frac{I_D - I_P}{t}.$$

However, this estimate of the source radiance includes both emitted and reflected radiation. To estimate the source temperature, the value of the emitted radiation alone needs to be known.

Goldman and coworkers (1983, pp.68-77) note that the contribution of reflected radiation can be significant. However, their data indicates that for an object with an emissivity of 0.9

in the temperature range considered here, reflected radiation accounts for approximately 5% of the source radiation. So, the value I_S found for the source radiation using the above equation reduced by 5% was used as the value for the emitted radiation, I_{ES}.

The temperature estimate based on the value I_{ES} was made using an iterative process. First, a temperature was assumed from which the percentage of radiation in the given band was found. Using this value, an emissivity value of 0.9, the value of I_{ES}, and the Stefan-Boltzmann Law; a new temperature was found. This process was repeated until the temperatures agreed. The results of this analysis are given in Table 4.

It should be noted here that these temperature estimates can not be regarded as true, measured values. No reliable temperature measurements of the bridge surface on the day of the radiance measurements were available for this study. For this reason, the radiance values were used to identify trends in the daily cycle of the bridge surface temperature. Identifying these trends was useful in determining appropriate environmental interactions to consider.

One Dimensional Model Results:

The finite-difference model using a five minute time-step and five layers was run for both the roadway and the piling. The

TABLE 4
ESTIMATED EMITTED RADAIANCE AND TEMPERATURE OF
THE DESTIN BRIDGE FROM 17 MAY 1984 DATA

TIME (HH:MM:SS)	PATH RAD.* $X10^5$	TRANS.	ROADWAY RAD.* & TEMP.			PILING RAD.* & TEMP.		
			APP. $X10^3$	SOURCE# $X10^3$	EST TEMP K	APP. $X10^3$	SOURCE# $X10^3$	EST TEMP K
05:26:45+	3	0.56	2.03	3.39	292	2.29	4.04	299
05:45:26+	3	0.56	2.05	3.43	293	2.30	4.05	299
06:05:21+	3	0.56	2.06	3.44	293	2.30	4.05	299
06:27:15	2.73	0.561	2.06	3.44	293	2.29	4.03	299
06:45:47	2.72	0.561	2.08	3.47	293	2.30	4.05	299
07:01:00	2.66	0.561	2.07	3.45	293	2.29	4.03	299
07:45:43	3.00	0.560	2.09	3.49	294	1.94	3.41	289
08:06:49	2.76	0.561	2.11	3.52	294	2.32	4.08	299
08:39:20	2.80	0.561	2.35	3.93	301	2.35	4.14	301
09:12:01	2.82	0.561	2.33	3.89	300	2.40	4.22	302
09:37:09	3.20	0.560	2.44	4.09	303	2.45	4.32	303
11:16:38	3.73	0.559	2.45	4.10	303	2.41	4.24	302
11:52:32	3.65	0.560	2.46	4.11	303	2.40	4.21	302
12:40:08	3.95	0.559	2.46	4.11	303	2.35	4.13	30!
13:37:36	3.42	0.561	2.75	4.61	310	2.33	4.10	300
14:08:20	3.61	0.560	2.80	4.68	311	2.32	4.07	300
15:07:28	4.08	0.559	2.77	4.64	311	2.32	4.08	300
16:42:44	3.44	0.561	2.64	4.42	308	2.33	4.10	300
17:08:26	4.10	0.559	2.61	4.37	306	2.38	4.19	301
18:12:10	4.83	0.557	2.44	4.08	303	2.33	4.09	300
18:36:13	4.79	0.557	2.40	4.01	301	2.33	4.09	300
18:49:00	4.81	0.557	2.41	4.03	302	2.35	4.13	301
19:27:10	3.91	0.559	2.30	3.84	299	2.32	4.08	300
19:52:44	3.38	0.560	2.22	3.72	297	2.30	4.05	299
21:39:48+	3	0.56	2.18	3.65	296	2.28	4.02	299

NOTES: *RADIANCES ARE IN WATTS/CM^2-SR MFASURED IN 7.35 to 11.9 MICROMETER BAND.
#SOURCE RADIANCES ARE REDUCED BY 5% TO ACCOUNT FOR REFLECTION.
+PATH RADIANCE AND TRANSMITTANCE FOR THESE TIMES ESTIMATED FROM TREND OF OTHER DATA.

thicknesses of the roadway and the piling are 7.5 inches and 24 inches respectively (see Appendix B). These models were run considering no reflected or emitted radiation from the water incident on the bridge structure. The reason for this approach is because of the trends identified from the estimated temperatures and the lower boundary sensitivity analysis.

The results of the model chosen are plotted in Figure 11, which also shows the estimated temperature data. This shows that the model predicts the piling becomes warmer than the roadway top surface at about the same time as indicated by the estimated
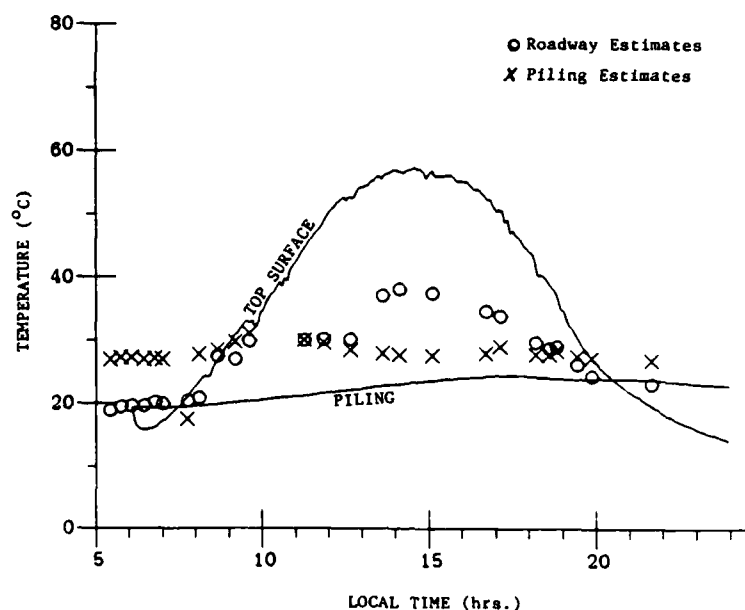
Figure 11. Roadway and Piling Surface Temperature Predictions (No Radiosity Incident on Lower Surface) Compared to Temperature Estimates.

temperature data. This was true even when emitted and reflected

radiation were considered. However, considering that no reflected

or emitted radiation was incident on the piling resulted in the

flat profile indicated by the estimated data. More variation in

the piling surface temperature was seen when emitted and reflected

radiation from the water were considered. The results using

reflected radiation only and both emitted and reflected radiation

on the lower surface are shown in Figures 12 and 13 respectively.
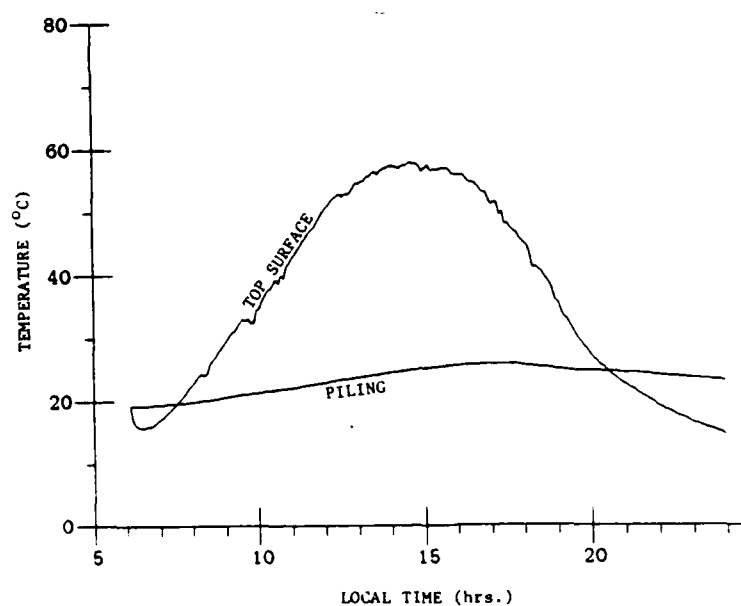
Figure 12. Roadway and Piling Surface Temperature Predictions
with Reflected Radiation only Incident on Lower Surface

45
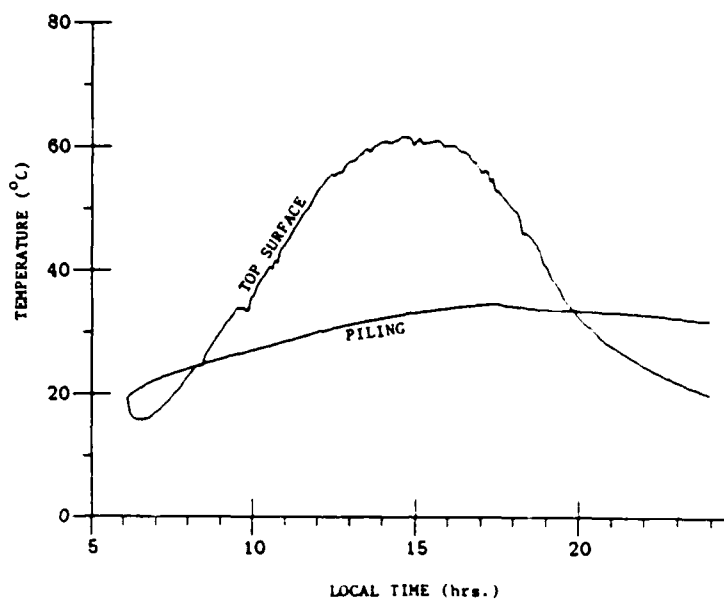
Figure 13.   Roadway and Piling Surface Temperature Prediction
with Emitted and Reflected Radiation Incident on
Lower Surface.

As noted in the sensitivity analysis, there is little
difference in the results for the top surface when both emitted
and reflected radiation are assumed incident on the lower
surface. Adding the effect of emitted and reflected radiation
drives the temperature of the piling nearly 15°C higher in the
late afternoon.

Two-Dimensional Model Results:

A two-dimensional, finite-difference model was developed in order to study the effects of side heating in both the east-west orientation of the Destin bridge and in a supposed north-south orientation. Both the roadway and the piling were modelled in two-dimensions, and a five minute time-step, as used with the one-dimensional model, was selected. The roadway is 48 ft. and 7.5 in. wide and the pilings are 2 ft. square (see Appendix B). Spacing for the roadway was five layers across the thickness like the one-dimensional model and 15 layers across the width. For the piling, five layers was again used across the thickness and the width was divided into 10 layers. This spacing produced cells of 0.0381 by 0.988 meters in the roadway and cells of 0.122 by 0.061 meters in the piling.

When modelled in an east-west direction, the two-dimensional roadway model shows that there is very little variation in the surface temperature across the width of the roadway. Table 5 shows the results of this model compared to the results of the one-dimensional model. From this it is seen that the temperature of the interior layers across the surface matches that predicted by the one-dimensional model. Only in the end layers and end surfaces is a slight difference seen.

TABLE 5
COMPARISON OF ROADWAY 1-D AND 2-D MODEL RESULTS

TEMPERATURES - °C

TIME	1-D	2-D							
7:07	17.52	17.60	17.52	17.52	17.52	17.52	17.52	17.52	17.60
8:07	23.25	23.31	23.25	23.25	23.25	23.25	23.25	23.25	23.31
9:07	30.19	30.16	30.19	30.19	30.19	30.19	30.19	30.19	30.16
10:07	35.74	35.56	35.74	35.74	35.74	35.74	35.74	35.74	35.56
11:07	43.25	42.89	43.25	43.25	43.25	43.25	43.25	43.25	42.89
12:07	50.71	50.13	50.71	50.71	50.71	50.71	50.71	50.71	50.13
13:07	54.40	53.55	54.40	54.40	54.40	54.40	54.40	54.40	53.55
14:07	56.75	55.61	56.75	56.75	56.75	56.75	56.75	56.75	55.61
15:07	56.82	55.40	56.81	56.82	56.82	56.82	56.82	56.81	55.40
16:07	55.08	53.45	55.07	55.08	55.08	55.08	55.08	55.07	53.45
17:07	50.69	48.93	50.67	50.69	50.69	50.69	50.69	50.67	48.93
18:07	43.69	41.83	43.67	43.69	43.69	43.69	43.69	43.67	41.83
19:07	33.25	31.39	33.23	33.25	33.25	33.25	33.25	33.23	31.39
20:07	25.73	24.08	25.70	25.73	25.73	25.73	25.73	25.70	24.08
21:07	21.34	19.89	21.31	21.34	21.34	21.34	21.34	21.31	19.89
22:07	18.06	16.85	18.04	18.06	18.06	18.06	18.06	18.04	16.85
23:07	15.72	14.78	15.69	15.72	15.72	15.72	15.72	15.69	14.78
23:57	14.02	13.27	14.00	14.02	14.02	14.02	14.02	14.00	13.27

NOTE: FIRST AND LAST 2-D TEMPERATURES ARE AT THE ENDS, 2ND AND 16TH TEMPERATURES ARE APPROXIMATELY ONE-HALF METER FROM ENDS. ALL OTHERS ARE APPROXIMATELY 1 METER APART.

As shown in Table 6, more variation is seen in the surface temperature of the piling when it is modelled in two dimensions. This was, of course, expected since the piling is a much smaller structure than the roadway. The center temperature, however, stays very close to that predicted by the one-dimensional model. Variations in temperature from the center to the ends are less than 2.5°C. Therefore, an average temperature across the surface of the piling would not be very different than that predicted by the one-dimensional model, indicating that a one-dimensional prediction could be used to evaluate the response of an infrared detector with reasonable accuracy.

Since the Destin Bridge runs east-west, the sides and the pilings underneath are subjected to a minimum of solar radiation However, for a bridge not oriented in an east-west direction, solar side heating could have a significant effect on the surface temperature. To investigate the effect of solar radiation on the sides and the piling, the two-dimensional models were run for the bridge as if it were at a north-south orientation.

The measurements of the solar radiation given in the weather data are for the radiation incident on a horitzontal surface. For the purpose of the north-south model, it was necessary to estimate the solar radiation incident on a vertical surface.

TABLE 6
COMPARISON OF PILING 1-D AND 2-D MODEL RESULTS

TIME	1-D	TEMPERATURES - $^{\circ}$C (2-D)											
7:07	19.31	19.38	19.33	19.32	19.31	19.31	19.31	19.31	19.31	19.31	19.32	19.33	19.38
8:07	19.53	19.79	19.62	19.55	19.53	19.53	19.53	19.53	19.53	19.53	19.55	19.62	19.79
9:07	20.07	20.77	20.36	20.14	20.09	20.07	20.07	20.07	20.07	20.09	20.14	20.36	20.77
10:07	20.58	21.56	21.11	20.76	20.63	20.59	20.58	20.58	20.59	20.63	20.76	21.11	21.56
11:07	21.10	22.39	21.89	21.41	21.21	21.13	21.11	21.11	21.13	21.21	21.41	21.89	22.39
12:07	21.73	23.50	22.81	22.19	21.92	21.80	21.76	21.76	21.80	21.92	22.19	22.81	23.50
13:07	22.40	24.50	23.76	23.03	22.67	22.51	22.45	22.45	22.51	22.67	23.03	23.76	24.50
14:07	23.00	25.32	24.61	23.80	23.38	23.17	23.09	23.09	23.17	23.38	23.80	24.61	25.32
15:07	23.60	26.10	25.42	24.56	24.08	23.83	23.73	23.73	23.83	24.08	24.56	25.42	26.10
16:07	24.05	26.65	26.01	25.15	24.63	24.36	24.24	24.24	24.36	24.63	25.15	26.01	26.65
17:07	24.40	27.02	26.45	25.62	25.09	24.78	24.65	24.65	24.78	25.09	25.62	26.45	27.02
18:07	24.25	26.28	26.14	25.52	25.02	24.71	24.57	24.57	24.71	25.02	25.52	26.14	26.28
19:07	23.88	25.48	25.47	25.09	24.69	24.40	24.26	24.26	24.40	24.69	25.09	25.47	25.48
20:07	23.94	25.57	25.41	25.08	24.76	24.51	24.37	24.37	24.51	24.76	25.08	25.41	25.57
21:07	23.81	25.19	25.14	24.90	24.62	24.41	24.29	24.29	24.41	24.62	24.90	25.14	25.19
22:07	23.49	24.45	24.61	24.49	24.28	24.10	24.00	24.00	24.10	24.28	24.49	24.61	24.45
23:07	23.09	23.73	23.95	23.97	23.85	23.71	23.63	23.63	23.71	23.85	23.97	23.95	23.73
23:57	22.78	23.21	23.45	23.56	23.50	23.40	23.33	23.33	23.40	23.50	23.56	23.45	23.21

NOTE: FIRST AND LAST 2-D TEMPERATURES ARE AT ENDS, 2ND AND 11TH TEMPERATURES ARE APPROXIMATELY 0.03 METERS FROM ENDS. ALL OTHERS ARE APPROXIMATELY 0.06 METERS APART.

To estimate the solar radiation incident on a vertical surface, it was noted that the measurements of the solar radiation were approximately sinusoidal with respect to the angle between the incoming radiation and the normal to the surface, peaking around mid-day when the sun would be directly overhead. It was assumed then that for a vertical surface the magnitude of the incident solar radiation would follow a cosine curve with respect to the same angle.

The sun was assumed to be directly overhead at a time halfway between the times of the first and last non-zero solar radiation measurements. Then the angle between the horitzontal surface normal and the solar radiation, Θ, was assumed to change at a constant rate. The magnitude of the solar radiation incident on a vertical surface was then estimated using the following equation:

$$W_{vert} = W_{sun} |\cos\Theta/\sin\Theta|.$$

It was assumed that the bridge structure would obscure solar radiation from the side of the piling facing inward. Therefore, two north-south piling models were used: one with the piling facing the morning sun and one facing the afternoon sun.

Table 7 shows a comparison of the one-dimensional model results to the results of modelling the roadway in a north-south direction. The north-south model was oriented so the left side

51

TABLE 7
COMPARISON OF ROADWAY 1-D AND N-S MODEL RESULTS

TEMPERATURES - °C

TIME	1-D	2-D								
7:07	17.52	19.92	17.52	17.52	17.52	17.52	17.52	17.52	17.52	17.60
8:07	23.25	26.79	23.27	23.25	23.25	23.25	23.25	23.25	23.25	23.31
9:07	30.19	33.90	30.22	30.19	30.19	30.19	30.19	30.19	30.19	30.16
10:07	35.74	39.23	35.77	35.74	35.74	35.74	35.74	35.74	35.74	35.56
11:07	43.25	46.42	43.30	43.25	43.25	43.25	43.25	43.25	43.25	42.89
12:07	50.71	53.27	50.77	50.71	50.71	50.71	50.71	50.71	50.71	50.13
13:07	54.40	56.10	54.46	54.40	54.40	54.40	54.40	54.40	54.40	53.58
14:07	56.75	57.67	56.81	56.76	56.75	56.75	56.75	56.75	56.75	55.86
15:07	56.82	57.08	56.87	56.82	56.82	56.82	56.82	56.82	56.82	56.07
16:07	55.08	54.82	55.13	55.08	55.08	55.08	55.08	55.08	55.08	54.76
17:07	50.69	50.05	50.73	50.69	50.69	50.69	50.69	50.69	50.68	51.10
18:07	43.69	42.72	43.72	43.69	43.69	43.69	43.69	43.69	43.69	45.19
19:07	33.25	32.11	33.27	33.25	33.25	33.25	33.25	33.25	33.26	36.27
20:07	25.73	24.66	25.74	25.73	25.73	25.73	25.73	25.73	25.75	28.63
21:07	21.34	20.37	21.35	21.34	21.34	21.34	21.34	21.34	21.37	23.58
22:07	18.06	17.23	18.07	18.06	18.06	18.06	18.06	18.06	18.10	19.79
23:07	15.72	15.07	15.72	15.72	17.72	17.72	15.72	15.72	15.75	17.03
23:57	14.02	13.51	14.02	14.02	14.02	14.02	14.02	14.02	14.06	15.14

NOTE: SEE NOTE TABLE 5

(corresponding to the 2-D temperatures on the left of Table 7)
faced the morning sun. Here, it is again seen that the interior
layer temperatures in the two-dimensional model match the
temperatures predicted by the one-dimensional model. However, the
effect of the solar side heating causes more difference between
the end and interior temperatures. This difference, though, is
still not significant in any of the interior layers.

Tables 8 and 9 show the results of modelling the piling as if
it faced the morning and afternoon sun respectively. The center
temperatures are in close agreement with those modelled with a
north-south oriented one-dimensional model, comparable to the
difference seen for the east-west orientation.

However, Tables 8 and 9 also show more variation between the
center and end temperatures. The variation is not significantly
higher, though, than that shown in Table 6 for the east-west
model. Table 8 indicates that in the morning for a piling facing
the morning sun the variation between the temperatures at the
center and at the ends is less than about five degrees Celsius.
This maximum occurs early at 8:07, and the center temperature is
higher than the end temperature where for the east-west model the
end was warmer than the center. This results from the piling
being warmed by the sun in the morning and that heat being
transferred to the surroundings more readily at the ends. In the

53

TABLE 8
COMPARISON OF PILING 1-D AND N-S MODEL RESULTS
FACING MORNING SUN

TIME	1-D						TEMPERATURES - $^{\circ}$C						
							2-D						
7:07	36.09	32.57	35.23	36.00	36.08	36.09	36.09	36.09	36.09	36.08	36.00	35.23	32.57
8:07	39.00	33.97	36.86	38.52	38.91	38.99	39.00	39.00	38.99	38.91	38.52	36.86	33.97
9:07	37.56	32.66	35.01	36.77	37.35	37.51	37.55	37.55	37.51	37.35	36.77	35.01	32.66
10:07	35.27	31.06	32.77	34.30	34.94	35.17	35.24	35.24	35.17	34.94	34.30	32.77	31.06
11:07	33.83	30.44	31.54	32.79	33.40	33.66	33.76	33.76	33.66	33.40	32.79	31.54	30.44
12:07	32.29	29.78	30.38	31.27	31.80	32.07	32.18	32.18	32.07	31.80	31.27	30.38	29.78
13:07	30.32	28.62	28.90	29.43	29.83	30.07	30.17	30.17	30.07	29.83	29.43	28.90	28.62
14:07	29.27	28.27	28.31	28.57	28.83	29.01	29.10	29.10	29.01	28.83	28.57	28.31	28.27
15:07	28.83	28.38	28.29	28.33	28.46	28.58	28.65	28.65	28.58	28.46	28.33	28.29	28.38
16:07	28.56	28.50	28.34	28.26	28.28	28.34	28.38	28.38	28.34	28.28	28.26	28.34	28.50
17:07	28.36	28.57	28.40	28.24	28.19	28.19	28.21	28.21	28.19	28.19	28.24	28.40	28.57
18:07	27.69	27.53	27.74	27.69	27.61	27.57	27.56	27.56	27.57	27.61	27.69	27.74	27.53
19:07	26.90	26.51	26.80	26.92	26.89	26.84	26.82	26.82	26.84	26.89	26.92	26.80	26.51
20:07	26.62	26.43	26.54	26.64	26.64	26.61	26.58	26.58	26.61	26.64	26.64	26.54	26.43
21:07	26.21	25.93	26.11	26.24	26.26	26.23	26.21	26.21	26.23	26.26	26.24	26.11	25.93
22:07	25.62	25.07	25.43	25.64	25.69	25.68	25.67	25.67	25.68	25.69	25.64	25.43	25.07
23:07	24.99	24.24	24.64	24.95	25.05	25.06	25.06	25.06	25.06	25.05	24.95	24.64	24.24
23:57	24.51	23.65	24.05	24.42	24.56	24.59	24.60	24.60	24.59	24.56	24.42	24.05	23.65

NOTE: SEE NOTE TABLE 6

TABLE 9
COMPARISON OF PILING 1-D AND N-S MODEL RESULTS
FACING AFTERNOON SUN

TIME	1-D	TEMPERATURES - $^\circ$C (2-D)											
7:07	19.31	19.38	19.33	19.32	19.31	19.31	19.31	19.31	19.31	19.31	19.32	19.33	19.38
8:07	19.53	19.79	19.62	19.55	19.53	19.53	19.53	19.53	19.53	19.53	19.55	19.62	19.79
9:07	20.07	20.77	20.36	20.14	20.09	20.07	20.07	20.07	20.07	20.09	20.14	20.36	20.77
10:07	20.58	21.56	21.11	20.76	20.63	20.59	20.58	20.58	20.59	20.63	20.76	21.11	21.56
11:07	21.10	22.39	21.89	21.41	21.21	21.13	21.11	21.11	21.13	21.21	21.41	21.89	22.39
12:07	21.73	23.50	22.81	22.19	21.92	21.80	21.76	21.76	21.80	21.92	22.19	22.81	23.50
13:07	22.60	24.69	23.97	23.24	22.88	22.72	22.66	22.66	22.72	22.88	23.24	23.97	24.69
14:07	24.86	26.91	26.40	25.65	25.23	25.02	24.95	24.95	25.02	25.23	25.65	26.40	26.91
15:07	27.96	29.69	29.51	28.87	28.43	28.20	28.10	28.10	28.20	28.43	28.87	29.51	29.69
16:07	32.00	33.05	33.33	32.95	32.55	32.30	32.19	32.19	32.30	32.55	32.95	33.33	33.05
17:07	36.83	36.78	37.71	37.73	37.43	37.19	37.07	37.07	37.19	37.43	37.73	37.71	36.78
18:07	43.01	40.73	42.97	43.72	43.61	43.42	43.31	43.31	43.42	43.61	43.72	42.97	40.73
19:07	49.85	44.61	48.36	50.13	50.36	50.27	50.18	50.18	50.27	50.36	50.13	48.36	44.61
20:07	42.01	36.59	39.54	41.77	42.35	42.41	42.37	42.37	42.41	42.35	41.77	39.54	36.59
21:07	35.04	31.14	32.76	34.52	35.21	35.38	35.40	35.40	35.38	35.21	34.52	32.76	31.14
22:07	31.67	28.31	29.59	31.03	31.71	31.95	32.01	32.01	31.95	31.71	31.03	29.59	28.31
23:07	29.52	26.42	27.53	28.80	29.45	29.73	29.82	29.82	29.73	29.45	28.80	27.53	26.42
23:57	28.22	25.32	26.28	27.46	28.09	28.39	28.49	28.49	28.39	28.09	27.46	26.28	25.32

NOTE: SEE NOTE TABLE 6

east-west model the surroundings are warmer than the piling so heat is transferred more readily to the ends. This difference decreases slowly until the ends become warmer than the piling at around 16:07.

Table 9 shows a slightly different scenario. The results for the north-south, afternoon sun facing model naturally follows the results of the east-west model in the morning. At 13:07, when the sun is starting to shine on the piling, the results start to become different. The center temperature starts to approach that of the end and is warmer by 17:07. After that, the cooling of the night-time is much like that for the east-west model.

One final comparison that can be made is to see if in a north-south orientation the piling would become warmer than the roadway, thereby being more of a target. Comparing Tables 7 and 8, it is seen that a piling facing the morning sun would be much warmer than the roadway until about mid-morning. Table 9 shows that a piling facing the afternoon sun would not become warmer than the roadway until very late in the afternoon, but it will stay much warmer than the roadway until late in the night. This is partly a result of the roadway losing much of its heat to the night sky while the piling is not subjected to this phenomena since it does not directly view the night sky.

It should be noted from Tables 5 and 6 that even when the piling is subjected to no solar radiation during the day it is warmer than the roadway late at night. However, being subjected to an afternoon sun causes the piling to become warmer than the roadway much sooner.

V. CONCLUSIONS AND REMARKS

This study has examined the numerical application of the Fourier heat equation to the problem of surface temperature prediction of a bridge-structure. The reason for approaching this problem was to provide a means for estimating the apparent contrast of a bridge using a Tactical Decision Aide model.

From the results of this study, several conclusions can be drawn. These are as follows:

1. Either a Runge-Kutta or a full finite-difference approximation provides nearly the same prediction of surface temperature.

2. A one-dimensional model provides nearly the same prediction as would a two-dimensional model.

3. The top surface temperature of a roadway structure is affected very little by the conditions of the lower surface.

4. The pilings of a bridge oriented in a north-south direction will provide a more visible target than the roadway in either the early morning or late afternoon, depending on what direction the piling faces.

5. Prediction of the roadway surface temperature is negligibly affected by orientation.

It was not possible in this study to determine the degree of accuracy to which the models predicted the surface temperatures. Trends in the variation of the surface temperature throughtout the day were approximately matched based on radiance measurements of a particular bridge. No reliable ground-truth data was available to compare to the predictions. More extensive measurements of a particular bridge or bridges, including both radiance measurements and temperature measurements, would be necessary to provide enough data to determine the accuracy of the predictions.

This study only considered the interaction of the bridge with a particular background--water. The effects of other backgrounds such as vegatation, rock, bare earth or various combinations should also be considered.

The use of different materials may also have an impact on the surface temperature prediction. The bridge that was the focus of this study was mostly concrete, and some consideration was given to the effect of steel reinforcements. Consideration should be given to a bridge which is mostly or all steel. Also, a wooden bridge should be considered from the standpoint that it may be a military target.

BIBLIOGRAPHY

BIBLIOGRAPHY

Burden, Richard L. and J. Douglas Faires. Numerical Analysis.
     Third Edition. Boston: Prindle, Weber & Schmidt, 1985.

Goldman, Robert B.; William R. Owens; Frank C. Greenwood; and
     Robert S. Hyde. Infrared Signature Analysis of Land Combat
     Vehicles and Environmental Backgrounds. Air Force Armament
     Laboratory, Eglin AFB, FL. AFATL-TR-83-18, 1983.

Kreith, Frank. Principles of Heat Transfer. Third Edition.
     New York: Intext Press, Inc., 1973.

Kreith, Frank and Jan F. Kreider. Principles of Solar Engineering.
     Washington: Hemisphere Publishing Corp., 1978.

Marlow, Steve. "CPM Validation Using 17 May 1984 Data."
     Unpublished Technical Memorandum 1900-39, Shalimar, FL:
     Analytics, Sensor Technology Division, 1986.

Rohsenow, Warren M. and James P. Hartnett. Handbook of Heat
     Transfer. New York: McGraw-Hill Book Co., 1973.

TABILS I, Target and Background Information Library System--Air to
     Ground IR Measurements. 17 May 1984 Data, Destin Bridge.
     Air Force Aramament Laboratory (AFATL/ASE), Eglin AFB, FL.

Thepchatri, Thaksin; C. Phillip Johnson; and Hudson Matlock.
     Prediction of Temperature and Streses in Highway Bridges by a
     Numerical Procedure Using Daily Weather Reports. Center for
     Highway Research, University of Texas at Austin, Austin, TX.
     CFHR 3-5-74-23, 1977.

Wachtmann, R. F.; G. J. Higgins; P. F. Hilton; D. B. Hodges; T. J.
     Keegan; B. A. Mareiro, Jr.; M. A. Mickelson; Ralph Shapiro;
     E. R. Talpey; C. N. Touart; and S. A. Wood. Operational
     Tactical Decision Aids--1985. Air Force Geophysics
     Laboratory, Hanscom AFB, MA. AFGL-TR-85-0186, 1985.

Wolfe, William L. and George J. Zissis. The Infrared Handbook.
     Washington: Office of Naval Research, Department of the
     Navy, 1978.

APPENDIXES

A. THERMOGRAPH SCENES OF THE DESTIN BRIDGE

Figure A-1 shown here contains thermograph scenes of the Destin Bridge taken on 17 May 1984 with an AGA 680 Thermovision Camera. These scenes are in the 7.0 to 14.0 micrometer band.
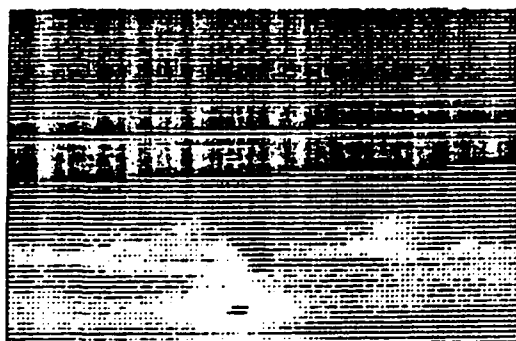
a. Scene at 5:27:40.

b. Scene at 5:46:24.

c. Scene at 6:46:36.
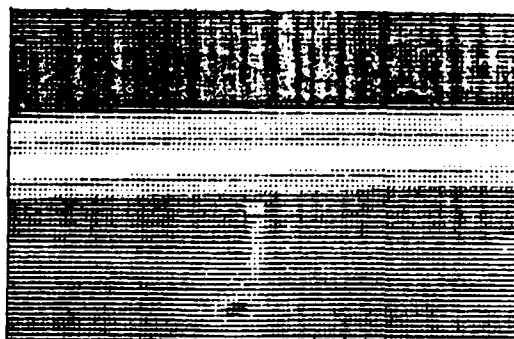
d. Scene at 9:13:01.

Figure A-1. Thermographs Scenes of the Destin Bridge.
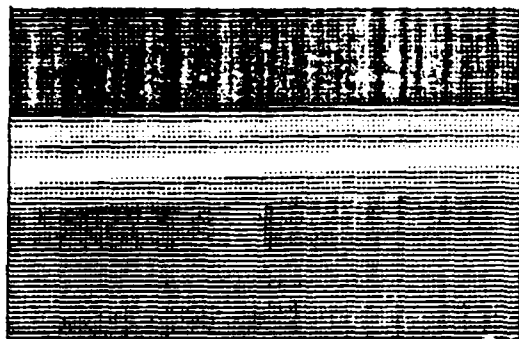
e. Scene at 11:53:08.
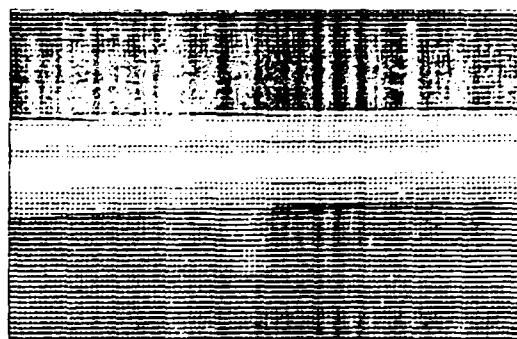
f. Scene at 15:08:30.
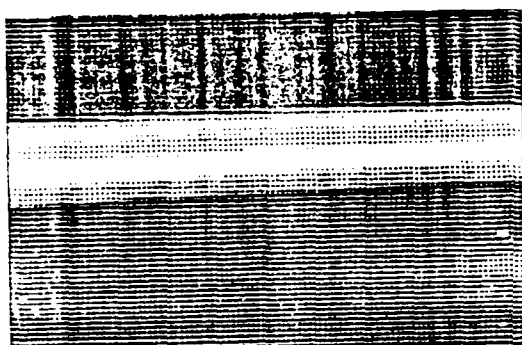
g. Scene at 18:36:53.
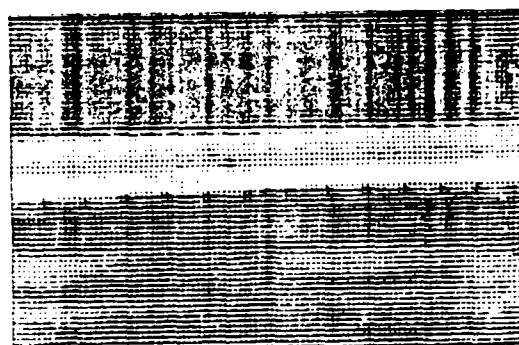
h. Scene at 19:28:13.

i. Scene at 20:39:26.

j. Scene at 21:09:59.

Figure A-1 (continued).

B. EXCERPTS FROM DRAWINGS OF DESTIN BRIDGE

Figures B-1 and B-2 are sections from engineering drawings of the Destin Bridge showing dimensions of parts of interest.
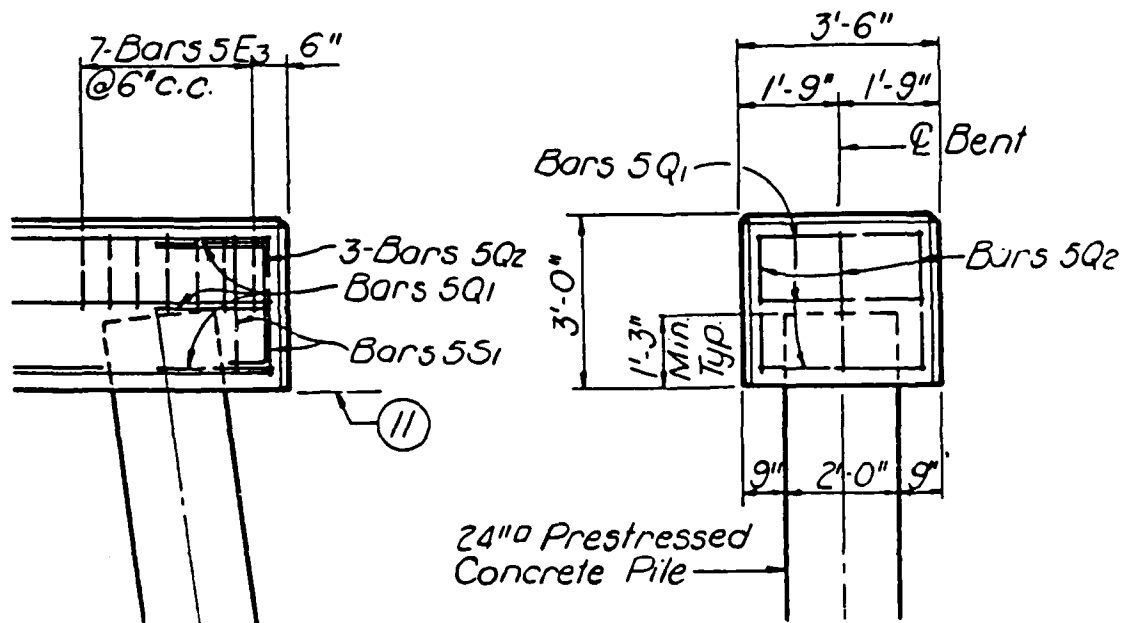
Figure B-1. Drawing Section Showing Piling Dimensions.

TYPICAL CROSS SECTION

SPANS NO. 1 THRU 28 & SPANS NO. 10 THRU 49

(Showing Location of Finished Grade Elevation Points)

Figure B-2. Drawing Section Showing Roadway Dimensions.

66

C. SAMPLE PROGRAM LISTINGS

```
C        * 1 MIN TIME STEP
C        * 5-LAYER MODEL
C        * FINITE DIFFERENCE APPROXIMATION
C        * REFLECTED & EMITTED RADIATION ON LOWER SURFACE
C
         DIMENSION TS(1074),T(5,1074),TL(1074)
         H=60.
         N=5
         JEND=1074
         ALPHA1=2.16*10.**(-7.0)
         ALPHA2=3.89*10.**(-7.0)
         ALPHA3=1.63*10.**(-6.0)
         ALPHA4=7.30*10.**(-7.0)
         ALPHA5=6.05*10.**(-7.0)
         ALPHA6=1.95*10.**(-8.0)
         EW=1.59*10.**(-4.0)
         SG=5.6697*10.**(-8.0)
         TM=21998
         IC=INT((1.+FLOAT(N))/2.)
         D=0.625/3.281
         D=D/FLOAT(N)
         A1=ALPHA1/D
         A2=ALPHA2/D
         A3=ALPHA3/D
         A4=ALPHA4/D
         A5=ALPHA5/D**2.
         A6=ALPHA6/D
         EW=EW/D
         TS(1)=19.25490
         DO 5 I=1,N
    5    T(I,1)=19.25490
         TL(1)=19.25490
         OPEN(UNIT=9,FILE='EWEATHR.DAT',FORM='FORMATTED',STATUS='OLD')
         OPEN(UNIT=10,FILE='TEMPRAD2.DAT',FORM='FORMATTED',STATUS='NEW')
         TMIN=H/60.
         WRITE(10,597)TMIN,N
  597    FORMAT(X,'FDIFF APPRX,',F5.1,' MIN TS,',I3,' LAYERS, FULL RAD'/)
         WRITE(10,598)
  598    FORMAT(X,'TIME',3X,'TEMPERATURES IN DEGREES C')
         WRITE(10,599)
  599    FORMAT(2X,'SEC',9X,'TS',10X,'TC',10X,'TL')
         DO 10 I=1,JEND-1
         WRITE(10,600)TM,TS(I),T(IC,I),TL(I)
  600    FORMAT(X,F6.0,5F12.5)
   99    READ(9,400)TI,VA,TA,WN,WY
  400    FORMAT(F7.0,F12.3,3F15.6)
         IF(TI.EQ.TM) GO TO 1
         GO TO 99
    1    WS=A1*WN+A2*(WY-SG*(TS(I)+273.15)**4.)+(A3+A4*VA)*(TA-TS(I))
         WL=(A3+A4*VA)*(TA-TL(I))+A2*(SG*((TA+273.15)**4.
     1   -(TL(I)+273.15)**4.))+A6*(WN+WY)+EW
         TS(I+1)=TS(I)+4.*A5*H*(T(1,I)-TS(I))+2.*H*WS
         T(1,I+1)=T(1,I)+A5*H*(T(2,I)-3.*T(1,I)+2.*TS(I))
         DO 6 J=2,N-1
    6    T(J,I+1)=T(J,I)+A5*H*(T(J+1,I)-2.*T(J,I)+T(J-1,I))
         T(N,I+1)=T(N,I)+A5*H*(2.*TL(I)-3.*T(N,I)+T(N-1,I))
         TL(I+1)=TL(I)+2.*H*WL+4.*A5*H*(T(N,I)-TL(I))
   10    TM=TM+H
         WRITE(10,600)TM,TS(JEND),T(IC,JEND),TL(JEND)
         CLOSE(UNIT=9)
         CLOSE(UNIT=10)
         STOP
         END
```

Figure C-1. Program Listing for 1-D Finite-Difference Model.

67

```fortran
C          * 15 MIN TIME STEP
C          * 3-LAYER MODEL
C          * RUNGE-KUTTA APPROXIMATION
      REAL K,KS,KL
      DIMENSION KS(4),K(3,4),KL(4),YS(72),Y(3,72),YL(72),T(3)
      H=900.
      N=3
      JEND=72
      ALPHA1=2.16*10.**(-7.0)
      ALPHA2=3.89*10.**(-7.0)
      ALPHA3=1.63*10.**(-6.0)
      ALPHA4=7.30*10.**(-7.0)
      ALPHA5=6.09*10.**(-7.0)
      ALPHA6=1.95*10.**(-7.0)
      SG=5.6697*10.**(-8.0)
      TM=21990.
      IC=INT((1.+FLOAT(N))/2.)
      D=0.625/3.281
      D=D/FLOAT(N)
      A1=ALPHA1/D
      A2=ALPHA2/D
      A3=ALPHA3/D
      A4=ALPHA4/D
      A5=ALPHA5/D**2.
      A6=ALPHA6/D
      TS=19.25490
      YS(1)=TS
      DO 5 I=1,N
      T(I)=19.25490
      Y(I,1)=T(I)
    5 TL=19.25490
      YL(1)=TL
      OPEN(UNIT=9,FILE='ENEATMP.DAT',FORM='FORMATTED',STATUS='OLD')
      OPEN(UNIT=10,FILE='RTEMP2.DAT',FORM='FORMATTED',STATUS='NEW')
      TMIN=H/60.
      WRITE(10,597)TMIN,N
  597 FORMAT(X,'R-K APPRX,',F5.1,' MIN TS,',I3,' LAYERS'/)
      WRITE(10,598)
  598 FORMAT(X,'TIME',5X,'TEMPERATURES IN DEGREES C')
      WRITE(10,599)
  599 FORMAT(2X,'SEC',9X,'TS',10X,'TC',10X,'TL')
      DO 20 I=1,JEND-1
      WRITE(10,600)TM,YS(I),Y(IC,I),YL(I)
  600 FORMAT(X,F6.0,3F12.5)
   99 READ(9,400)TI,VA,TA,WN,WY
  400 FORMAT(F7.0,F12.3,3F15.6)
      IF(TI.EQ.TM) GO TO 1
      GO TO 99
    1 X=2.
      DO 10 L=1,4
      KS=A1*WN+A2*(WY-SG*(TS+273.15)**4.)+(A3+A4*VA)*(TA-TS)
      KL=(A3+A4*VA)*(TA-TL)+A2*(SG*((TA+273.15)**4.
     1-(TL+273.15)**4.))+A6*(WN+WY)
      KS(L)=(4.*A5*(T(1)-TS)+2.*KS)*H
      K(1,L)=(A5*(T(2)-3.*T(1)+2.*TS))*H
      DO 15 J=2,N-1
   15 K(J,L)=(A5*(T(J+1)-2.*T(J)+T(J-1)))*H
      K(N,L)=(A5*(2.*TL-3.*T(N)+T(N-1)))*H
      KL(L)=(2.*KL+4.*A5*(T(N)-TL))*H
      IF(L.LT.3) GO TO 3
      X=1.
    3 TS=YS(I)+KS(L)/X
      DO 16 M=1,N
   16 T(M)=Y(M,I)+K(M,L)/X
   10 TL=YL(I)+KL(L)/X
      YS(I+1)=YS(I)+(KS(1)+2.*KS(2)+2.*KS(3)+KS(4))/6.


      DO 17 J=1,N
   17 Y(J,I+1)=Y(J,I)+(K(J,1)+2.*K(J,2)+2.*K(J,3)+K(J,4))/6.
      YL(I+1)=YL(I)+(KL(1)+2.*KL(2)+2.*KL(3)+KL(4))/6.
      TS=YS(I+1)
      DO 18 J=1,N
   18 T(J)=Y(J,I+1)
      TL=YL(I+1)
   20 TM=TM+H
      WRITE(10,600)TM,YS(JEND),Y(IC,JEND),YL(JEND)
      CLOSE(UNIT=9)
      CLOSE(UNIT=10)
      STOP
      END
```

Figure C-2. Program Listing for 1-D Runge-Kutta Model.

```
C        * 2-D FINITE DIFFERENCE APPROXIMATION
C        * 5 MINUTE TIME STEP
C        * 5 LAYERS IN X
C        * 15 LAYERS IN Y
C        * NORTH-SOUTH ORIENTATION
C
      DIMENSION T(7,17),XK(7,17),YK(7,17)
      ALPHA1=2.16*10.**(-7.0)
      ALPHA2=3.89*10.**(-7.0)
      ALPHA3=1.63*10.**(-9.0)
      ALPHA4=7.30*10.**(-7.0)
      ALPHA5=6.05*10.**(-7.0)
      SG=5.6697*10.**(-8.0)
      TM=21996.
      DX=(0.625/3.281)/5.
      A1X=ALPHA1/DX
      A2X=ALPHA2/DX
      A3X=ALPHA3/DX
      A4X=ALPHA4/DX
      A5X=ALPHA5/DX**2.
      DY=(48.625/3.281)/15.
      A1Y=ALPHA1/DY
      A2Y=ALPHA2/DY
      A3Y=ALPHA3/DY
      A4Y=ALPHA4/DY
      A5Y=ALPHA5/DY**2.
      H=300.
      THETA=(90./23770.)*(TM-21738.)
      DTHETA=H*90./23770.
      DO 5 I=1,7
      DO 5 J=1,17
    5 T(I,J)=19.25490
      OPEN(UNIT=9,FILE='WEATHR.DAT',FORM='FORMATTED',STATUS='OLD')
      OPEN(UNIT=10,FILE='NSTEMP.DAT',FORM='FORMATTED',STATUS='NEW')
      WRITE(10,599)
  599 FORMAT(X,' N-S BRIDGE SURFACE TEMPERATURES - 5 MIN TS - 5 X 15 LAY
     1ERS'/)
      DO 30 K=2,215
   99 READ(9,400)TM1,VA,TA,WN,WY
  400 FORMAT(F7.0,F12.3,3F15.6)
      IF(TM1.EQ.TM) GO TO 1
      GO TO 99
    1 DO 20 J=1,17
      WSX=A1X*WN+A2X*(WY-SG*(T(1,J)+273.15)**4.)+(A3X+A4X*VA)*
     1(TA-T(1,J))
      WLX=(A3X+A4X*VA)*(TA-T(7,J))+A2X*SG*((TA+273.15)**4.
     1-(T(7,J)+273.15)**4.)
      XK(1,J)=4.*A5X*H*(T(2,J)-T(1,J))+2.*H*WSX
      XK(2,J)=A5X*H*(T(3,J)-3.*T(2,J)+2.*T(1,J))
      DO 40 I=3,5
   40 XK(I,J)=A5X*H*(T(I+1,J)-2.*T(I,J)+T(I-1,J))
      XK(6,J)=A5X*H*(2.*T(7,J)-3.*T(6,J)+T(5,J))
   20 XK(7,J)=4.*A5X*H*(T(6,J)-T(7,J))+2.*H*WLX
      WNV=COSD(THETA)*WN/SIND(THETA)
      DO 25 I=1,7
      X=1.
      IF(THETA.GT.90) X=0.
      WSY=A1Y*WNV*X+(A3Y+A4Y*VA)*(TA-T(1,1))+A2Y*SG*((TA+273.15)**4.
     1-(T(I,1)+273.15)**4.)
      X=1.
      IF(THETA.LT.90) X=0.
      WLY=A1Y*WNV*X+(A3Y+A4Y*VA)*(TA-T(1,17))+A2Y*SG*((TA+273.15)**4.
     1-(T(I,17)+273.15)**4.)
      YK(I,1)=4.*A5Y*H*(T(I,2)-T(1,1))+2.*H*WSY
      YK(I,2)=A5Y*H*(T(I,3)-3.*T(I,2)+2.*T(1,1))
      DO 24 J=3,15
   24 YK(I,J)=A5Y*H*(T(I,J+1)-2.*T(I,J)+T(I,J-1))
      YK(I,16)=A5Y*H*(2.*T(I,17)-3.*T(I,16)+T(I,15))
   25 YK(I,17)=4.*A5Y*H*(T(I,16)-T(I,17))+2.*H*WLY
      DO 26 I=1,7
      DO 26 J=1,17
   26 T(I,J)=T(I,J)+XK(I,J)+YK(I,J)
      TM=TM+H
      THETA=THETA+DTHETA
   30 WRITE(10,600)TM,T(1,1),T(1,2),T(1,3),T(1,4),T(1,5),T(1,9),
     1T(1,13),T(1,14),T(1,15),T(1,16),T(1,17)
  600 FORMAT(F7.0,11F8.2)
  999 CLOSE(UNIT=9)
      CLOSE(UNIT=10)
      STOP
      END
```

Figure C-3. Program Listing for 2-D Finite-Difference Model.

69

Paul Terry Cross, ███ ████████████ ██ ██ ████████████

PII Redacted

T████████ He attended various elementary schools in Marshall

County and in 1976 graduated from Marshall County Senior High

School in Lewisburg. He entered Tennessee Technological University

in the fall of the same year and in June 1981 received a Bachelor

of Science degree in Engineering Science and Mechanics.

Also in June 1981, the author entered the U. S. Air Force and

was sent to the Officer Training School at Lackland AFB, TX with

subsequent assignment to the Aeronautical Systems Division at

Wright-Patterson AFB, OH. In 1984, he was selected for an Air

Force sponsored graduate education program in aerospace engineering and

entered The University of Tennessee Space Institute in September

1985. Upon completion of this program, he will be assigned to the

Air Force Flight Test Center at Edwards AFB, CA.